Learning hydrodynamic coefficient databases for vortex induced vibration prediction of marine risers using sparse sensor measurements

by
Andreas P. Mentzelopoulos
B.S.E. Mechanical Engineering, University of Michigan (2020)
B.S.E. Naval Architecture & Marine Engineering, University of Michigan (2020)
Submitted to the Department of Mechanical Engineering
in partial fulfillment of the requirements for the degree of
Master of Science in Mechanical Engineering
at the
MASSACHUSETTS INSTITUTE OF TECHNOLOGY
May 2022

Author .....
Department of Mechanical Engineering
May 6, 2022

Certified by .....
Michael S. Triantafyllou
Henry L. and Grace Doherty Professor in Ocean Science and Engineering; Professor of Mechanical and Ocean Engineering; Director, MIT Sea Grant
Thesis Supervisor

Certified by .....
Themistoklis Sapsis
Professor of Mechanical and Ocean Engineering
Thesis Supervisor

Accepted by .....
Nicolas Hadjiconstantinou
Professor; Co-Director, Center for Computational Science and Engineering; Associate Director, Center for Exascale Simulation of Materials in Extreme Environments; Graduate Officer

Learning hydrodynamic coefficient databases for vortex induced vibration prediction of marine risers using sparse sensor measurements

by

Andreas P. Mentzelopoulos

Submitted to the Department of Mechanical Engineering
on May 6, 2022, in partial fulfillment of the
requirements for the degree of
Master of Science in Mechanical Engineering

Abstract

Semi-empirical models are currently the state-of-the-art technology for flexible cylinder vortex induced vibrations (VIV) predictive modelling. Accurate prediction of the structural response relies heavily on the accuracy of the acquired hydrodynamic coefficient database. Due to the large number of inputs required, the construction of systematic hydrodynamic coefficient databases from rigid cylinder forced vibration experiments can be time-consuming or even intractable. An alternative approach has been implemented in this work to improve the flexible cylinder VIV prediction by machine-learning optimal parametric hydrodynamic databases using physical measurements along the structure. The methodology is applied to a straight riser in uniform flow and extended to non-straight riser configurations and non-uniform incoming flow profiles. Moreover, database inference is extended to using direct sparse sensor measurements along the structure. Specifically, a 19-dimensional parametric hydrodynamic coefficient database is obtained for: (i) straight riser in uniform flow (using either displacement or strain data) (ii) straight riser in stepped uniform flow (iii) straight riser in sheared flow (iv) catenary riser in uniform flow of various incidence directions between the catenary plane and the incoming flow stream (v) stepped (2-diameter) riser in uniform flow. The predicted amplitude and frequency responses, using the extracted databases, are compared with observed experimental results.

Thesis Supervisor: Michael S. Triantafyllou
Title: Henry L. and Grace Doherty Professor in Ocean Science and Engineering; Professor of Mechanical and Ocean Engineering; Director, MIT Sea Grant

Thesis Supervisor: Themistoklis Sapsis
Title: Professor of Mechanical and Ocean Engineering

The future emerges from the past.

Dedicated, with love, to my forefathers and foremothers, of blood and of intellect.

Acknowledgments

I would first like to share the following, from Ἰθάκη (Ithaca).

Σὰ βγεῖς στὸν πηγαιμὸ γιὰ τὴν Ἰθάκη,
νὰ εὔχεσαι νᾶναι μακρὺς ὁ δρόμος,
γεμάτος περιπέτειες, γεμάτος γνώσεις.
[...]
Τοὺς Λαιστρυγόνας καὶ τοὺς Κύκλωπας,
τὸν ἄγριο Ποσειδώνα δὲν θὰ συναντήσεις,
ἂν δὲν τοὺς κουβανεῖς μὲς στὴν ψυχή σου,
ἂν ἡ ψυχή σου δὲν τοὺς στήνει ἐμπρός σου.
[...]
Πάντα στὸ νοῦ σου νἄχῃς τὴν Ἰθάκη.
Τὸ φθάσιμον ἐκεῖ εἶν᾽ ὁ προορισμός σου.

Ἀλλὰ μὴ βιάζῃς τὸ ταξείδι διόλου.
Καλλίτερα χρόνια πολλὰ νὰ διαρκέσει.
Καὶ γέρος πιὰ ν᾽ ἀράξῃς στὸ νησί,
πλούσιος μὲ ὅσα κέρδισες στὸν δρόμο,
μὴ προσδοκώντας πλούτη νὰ σὲ δώσῃ ἡ
Ἰθάκη.

Ἡ Ἰθάκη σ᾽ ἔδωσε τ᾽ ὡραῖο ταξίδι.
[...]

-Κωνσταντῖνος Καβάφης (1863-1933).

As you set out for Ithaka,
hope the journey is a long one,
full of adventure, full of knowledge.
[...]
Not the Laestrygonians or the Cyclops,
nor the fierce Poseidon will you encounter,
unless you're bearing them within your soul, unless your soul sets them up before you.[...]
Always keep Ithaca in mind.
Arriving there is your bourne.

But don't hurry the journey at all.
Better if it lasts for many years.
At last you'll anchor at the island old,
wealthy with all you 've gained along the way, not expecting that Ithaca will give you riches.

Ithaka has given you the marvelous journey.[...]

- Konstantinos Kavafis (1863-1933).

"If I have seen (a little) further, it is by standing on the shoulders of giants". Writing this means that the dream of a ten year old boy has finally come true. This work reflects not only two years of research but also the efforts of a kid, a teenager, and a young adult for more than a decade.

It goes without saying, that I am indebted to my advisors, Professor Michael S. Triantafyllou and Professor Themis Sapsis, for guiding me in the pursuit of knowledge and truth. I am humbled to have worked alongside researchers of their caliber.

I would further like to extend my gratitude to Professor Michael M. Bernitsas, who offered me the chance to engage in research as an undergraduate at the University of Michigan. Having worked alongside such an inspiring researcher and teacher, I will always have someone to look up to.

I am grateful to have crossed paths with my colleague and friend, Professor Dixia Fan, during his time at MIT. I am truly indebted to him for his support and mentorship. Without his invaluable guidance and contributions, this work wouldn't have been possible.

I would also like to thank my lab-mates and friends, Jose and Sam, not only for their contributions to this work, but also for the good times we spent together.

Celebrating the beauty of music, I would like to thank Maestro Adam K. Boyles of the MIT Symphony Orchestra, who revived a dying -then- but flourishing -now-, musical spirit. Bereft of art, life would be without colour; Maestro Boyles has generously provided colours - the most *vivid* - to my palette these past two years.

Remembering where the journey started, I would also like to acknowledge my high school chemistry teacher, Konstantinos Komninos, for his, in my humble opinion, exceptional moral character and teaching skills. I wish him well.

Further, I would like to extend my gratitude to a person who shaped my character in many ways, a true pedagogue, Maestra Nina Patrikidou of the Youth Symphony Orchestra under the auspices of the National Radio and Television (ERT, third programme) of Greece.

"Life is suffering". To my brother, George, my sister, Anna, and all those, my *friends*, some of twenty years and others of twenty months, who helped me carry the stone

and took some of its weight off my shoulders, I thank you deeply.

Finally and most importantly, I would like to thank my greatest teachers and the grandest giants of them all, my loving parents, Panos Mentzelopoulos and Theodora Sfantou. I truly couldn't have been luckier to have you by my side. For making me believe in dreaming and reminding me that *"if you don't find Spring, you'll have to make it"*, I thank you with all my heart.

Contents

List of Figures

List of Tables

Chapter 1

Introduction

1.1 Vortex induced vibrations (VIV)

Vortex induced vibrations (VIV) have been known to engineers for more than 400 years, first observed by the ancient Greeks as "aeolian tones", sounds created by wake-eddy vortex induced pressure fluctuations as wind passes around obstacles and later sketched as vortices by Leonardo da Vinci. Extensive studies on the subject have been conducted in the last five decades in order to mainly suppress VIV due to their destructive capabilities[23, 5, 1], although attempts to harness energy from flows have also led to their study[6, 21, 19, 3].

VIV affect bluff bodies in the presence of currents due to periodic irregularities developed in the bodies' wakes. Those irregularities (vortices) create an alternating pressure variation which synchronizes with body motion creating consistent vibrations which may have detrimental effects on engineered structures by causing direct failure or extensive fatigue damage[4].

VIV occur across a wide range of body oscillating frequencies, known as the lock-in range, in which synchronization between vortex shedding and body motion is eminent[39, 33]. Some have described this synchronization, mainly enabled by the variability of the added mass, as a nonlinear resonance given its broad-banded nature[16]. During lock-in, moderate response amplitudes occur, typically self-limited to about one diameter. The vortex shedding frequency can differ from the Strouhal

frequency of a fixed cylinder because, as work via flow visualization has revealed, the relative motion between the vibrating cylinder and the shed vortices can significantly alter the effective fluid added mass[35], resulting in a variable natural frequency as a function of the stream velocity[37].

Given the bluff shape of many modern offshore engineering equipment, such as cables, mooring lines, marine risers, and others, a thorough understanding of the underlying physics of VIV is essential in controlling their effects, be they fatigue damage to offshore equipment or energy harnessed from flows[6, 2].

1.2 Rigid and flexible body VIV

Through experimental[18, 24, 41, 12] and numerical[11, 40, 36, 9, 10, 25] methods, studies reveal that the hydrodynamic forcing on cylinders can vary significantly as the incoming flow stream velocity and the cylinder motions change. Specifically, the forcing seems to be greatly affected by the vortex shedding pattern.

Some of the first attempts to study VIV were experiments in which a rigid cylinder was forced to oscillate in a prescribed trajectory[28]. In particular, studies focused on the mean drag coefficient C_d, the lift coefficient in-phase with the velocity C_{lv}, and the added mass coefficient in the cross-flow (CF) direction, C_m, as functions of the true reduced velocity $V_r = \frac{U}{fD}$ and the non-dimensional CF amplitude $A^* = \frac{A}{D}$, where U is the prescribed fluid velocity; f is the prescribed motion frequency; A is the prescribed motion amplitude; and D is the cylinder's diameter[15, 29, 12]. The experiments revealed that regions of positive C_{lv}, denoting net energy transferred from the fluid to the structure, were constrained to a specific range of V_r and A^*. In addition, they reported that the added mass coefficient could vary significantly assuming both negative and positive values around the true reduced velocity value of $V_r = 5.9$.

The measured hydrodynamic coefficients from rigid cylinder forced vibration experiments were later successfully used to predict the motions of rigid cylinder VIV[34], and they have served as hydrodynamic coefficient databases used to accurately predict

the fluid forces in semi-empirical flexible riser VIV prediction codes[26, 31, 20].

VIV of flexible bodies are similar to those of rigid bodies in the sense that the driving mechanism (the vortices) is the same; the key difference is that the motion and forcing are not spanwise uniform for flexible bodies. Thus, predicting the flexible body response is significantly more challenging. Studies have been conducted to investigate the flow structure interaction of flexible bodies in VIV and revealed very complex behaviors, including various structural modes, responses of traveling waves, and recently multi-modal as well as multi-frequency vibrations[13]. Insights on the flow past the bodies' wakes, in which boundary layers, shear layers, vortices, and the bodies themselves interact, are currently being reported[14, 17].

1.3 The added mass and lift coefficients

The intuitive way of thinking of the added mass is as "the entrained fluid mass" disturbed by the trajectory of a body moving through the fluid. However, in VIV the nature of the added mass is rather elusive and more complex. The added mass represents the component of the forcing on the body which is in anti-phase with acceleration, thus appearing as an added mass term in the equations of motion. Albeit named added mass, in VIV the quantity may assume both positive and negative values[14, 22].

The sign of the added mass strongly depends on the timing of the vortex shedding and a phenomenon known as the wake capture. The motion always initiates at the Strouhal frequency and then, due to the vortex formation in the wake, drifts slightly from it as it tries to match the natural frequency of the structure (as defined by the added mass)[30]. Since vortices are low pressure areas, the timing of vortex formation alters the suction force caused by the vortex on the body. If the suction force is in the direction of the body's acceleration it will reduce the inertia force resulting in a reduced added mass; if the suction force opposes the body's acceleration the apparent added mass increases.

There also seems to be a strong correlation between the vortex shedding mode

and the value of the added mass. Multiple vortex shedding modes have been reported in literature[42, 38] such as "2S", "2P", "P+S", "2P+2S", and others. For example, a "2S" shedding mode, that is two single vortices shed per period, is associated with a positive added mass while a "2P" shedding mode, which is two pairs of vortices shed, is associated with a negative added mass[35].

The lift coefficient in phase with velocity is important in the fact that it relates the amplitude of vibration with the frequency. The strong dependence of the amplitude of motion to the C_{lv} makes the coefficient particularly significant as it indirectly governs the strain and thus the fatigue of bodies affected by VIV. Both the strain and the fatigue are of critical importance in determining equipment design parameters and estimating service life. Finally, as stated earlier, the sign of the lift coefficient provides insight in the direction of energy transfer in the coupled flow-structure interaction problem, i.e. from fluid to structure or vice versa.

1.4 Motivation

Semi-empirical models and prediction programs serve as the current state-of-the-art technology for VIV prediction[31, 20, 32]. Among several parameters, estimation of the hydrodynamic coefficients, such as the added mass coefficient C_m and the lift coefficient in phase with velocity C_{lv}, is key to the accurate prediction of the body's response using semi-empirical models. The hydrodynamic database serves as a mapping between the nondimensional amplitude, the nondimensional frequency, and the added mass and lift coefficients.

Estimating the hydrodynamic coefficients is a nontrivial process that requires performing many forced-vibration experiments with rigid cylinders, a process very expensive as well as time consuming. In addition, due to the wide input parametric space, using brute-force experiments to obtain a general hydrodynamic database, suitable for risers of various geometries in various flow conditions, is an impossible task.

Although at first glance computational fluid dynamics simulations may sounds

like a viable option to replace experiments, given the high Reynolds number as well as the length scale of the field problem of risers (spanning kilometers with length to diameter ratios $L/D \approx O(10^4)$ at Reynolds numbers $Re \approx O(10^5)$) resolving full scale riser simulations would take months on the fastest supercomputers at low Reynolds numbers and have never been done at high Reynolds numbers to the best of the author's knowledge. There exists thus a need for developing *a new methodology to study VIV in a consistent and efficient manner.*

An alternative computational approach to studying VIV by obtaining the hydrodynamic coefficient database from data was recently proposed. This work explores and extends the new paradigm[27] of the hydrodynamic database inference directly from the flexible body's response: an optimized parametric hydrodynamic database obtained from the comparison between experimental and semi-empirical code prediction results which could achieve a significant improvement in the predictive accuracy of semi-empirical models.

Although the proposed methodology outlined in this work may be extended to any flexible body undergoing VIV, it was inspired by the marine riser vortex induced vibration problem. The riser serves as the lifeline between a deep sea rig and the offshore platform; VIV induce cyclic loads to risers and constantly fatigue them. An adequate understanding of the riser response can provide insights to the true fatigue damage and ensure safe operation of the riser, preventing the possibly catastrophic event of riser failure.

Chapter 2

Methods

This section outlines the modelling and learning problem formulation of the hydrodynamic database coefficient inference method. The optimization routine is also presented.

2.1 Modelling flexible body VIV

The flexible body undergoing VIV is modeled as a tensioned flexible continuous-mass vibrating under the excitation of a hydrodynamic force[31, 43].

2.1.1 Eigenvalue problem

Consider a flexible body differential element of mass $\Delta\mu$ at an arbitrary orientation (defined by an angle θ) with respect to the x-y axes as shown in Figure 2-1. The following forces and moments act on the element: (1) tension, (2) shear forces, (3) bending moments, (4) the hydrodynamic force, and (5) a damping force. Then, the equation of motion in the y (CF) direction is:

$$\Sigma F_y = \Delta\mu \frac{\partial^2 y}{\partial t^2} \tag{2.1}$$

$$(Vcos\theta)_{x+\Delta x} - (Vcos\theta)_x + (Tsin\theta)_{x+\Delta x} - (Tsin\theta)_x + F - F_b = \Delta\mu \frac{\partial^2 y}{\partial t^2} \tag{2.2}$$

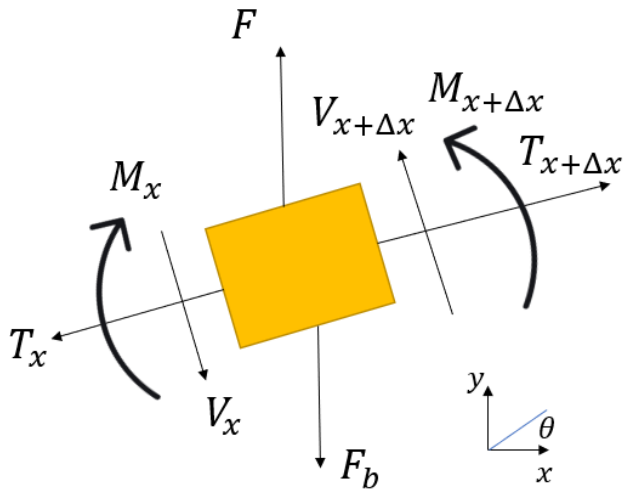

Figure 2-1: Flexible body differential element

$$\frac{\partial}{\partial x}(Vcos\theta)\Delta x + \frac{\partial}{\partial x}(Tsin\theta)\Delta x + F - F_b = \Delta\mu\frac{\partial^2 y}{\partial t^2} \tag{2.3}$$

Recognizing how $\Delta\mu = m\Delta x$, where m is mass per unit length and linearizing (since the amplitude is no greater than one diameter) $sin\theta \approx \theta \approx \frac{\partial y}{\partial x}$ and $cos\theta \approx 1$, we arrive at

$$\frac{\partial V}{\partial x}\Delta x + \frac{\partial}{\partial x}(T\frac{\partial y}{\partial x})\Delta x + F - F_b = m\Delta x\frac{\partial^2 y}{\partial t^2} \tag{2.4}$$

Rearranging and letting $F = f \cdot \Delta x$ and $F_b = f_b \cdot \Delta x$ where f and f_b are the hydrodynamic and damping forces per unit length, respectively, we arrive at

$$m\frac{\partial^2 y}{\partial t^2} + f_b - \frac{\partial V}{\partial x} - \frac{\partial}{\partial x}(T\frac{\partial y}{\partial x}) = f \tag{2.5}$$

At this point we take into account the following relation which is true assuming that the element has negligible rotary inertia. The expression also relates the curvature (to first order) using Euler's constitutive relation $M = EI\frac{\partial^2 y}{\partial x^2}$ with the bending moment.

$$-\frac{\partial V}{\partial x} = \frac{\partial^2 M}{\partial x^2} = \frac{\partial^2}{\partial x^2}(EI\frac{\partial^2 y}{\partial x^2}) \tag{2.6}$$

Finally, combining 2.4 with 2.6 and replacing the damping force with $f_b = b\frac{\partial y}{\partial t}$, we arrive at the complete equation of motion describing the coupled flow-structure interaction for the flexible body:

$$m\frac{\partial^2 y}{\partial t^2} + b\frac{\partial y}{\partial t} - \frac{\partial}{\partial x}(T\frac{\partial y}{\partial x}) + \frac{\partial^2}{\partial x^2}(EI\frac{\partial^2 y}{\partial x^2}) = f \tag{2.7}$$

where m is the mass per unit length, b is the damping, T is the tension on the section (and a function of the span), EI is the flexural rigidity of the body (also function of span), and f is the hydrodynamic force. The dimensions of Equation 2.7 are force per unit length. We are interested in determining normal modes of vibration which are sinusoidal in time assuming the following form.

$$y(x,t) = Re\left[Y(x)e^{i\omega t}\right] \tag{2.8}$$

where $Y(x)$ is the complex valued amplitude of vibration along the span and ω is the cyclic frequency of vibration. The hydrodynamic force is assumed to have the following form, corresponding to a component in anti-phase with acceleration (the added mass force) and a component in phase with velocity as shown below.

$$f = Re\left[\left(\frac{1}{4}C_m\pi\rho D^2\omega^2 Y + i\frac{1}{2}C_{lv}\rho U^2 D\frac{Y}{|Y|}\right)e^{i\omega t}\right] \tag{2.9}$$

where Re means the "real part" (not to be confused with Reynolds number), ρ is the fluid-density, D is the body's diameter, and U is the stream velocity (assumed time invariant). The hydrodynamic coefficients C_m and C_{lv} are introduced to the model in the hydrodynamic force and their dependence on ω and Y is assumed known a priori. The term $Y/|Y|$ ensures that the excitation force remains in phase with velocity and

has manitude 1. It should be noted that the hydrodynamic force f, (which drives the motion) depends on the amplitude of the response Y as well as the frequency ω.

Trivial manipulation of equations 2.7, 2.8 and 2.9 leads to the following eigenvalue problem (EVP) which may be used to determine the frequency and mode shape of the riser free vibration, i.e. under the excitation of hydrodynamic forcing only.

$$\frac{d^2}{dx^2}(EI\frac{d^2Y}{dx^2}) - \frac{d}{dx}(T\frac{dY}{dx}) + \left[-(m+\alpha C_m)\omega^2 + ib\omega\right] Y = iC_{lv}qD\frac{Y}{|Y|} \tag{2.10}$$

where $\alpha = \frac{1}{4}\rho\pi D^2$, and $q = \frac{1}{2}\rho U^2$. Given appropriate boundary conditions for the amplitude $Y(x)$ (pinned, fixed, etc.), Equation 2.10 is a well defined nonlinear eigenvalue problem. The nonlinearity originating from the dependence of the hydrodynamic coefficients C_m and C_{lv} to the amplitude $Y(x)$ and the vibration frequency ω which in general is nonlinear. It should be noted that for this coupled fluid/structure interaction problem the vibration modes are not necessarily orthogonal to each other, and solutions are only unique up to a constant phase.

Solving the EVP is a rather nontrivial process which may be done using an iterative nonlinear numerical solver. For the purpose of this work, the solver VIVA™ which has been developed by Professor M. S. Triantafyllou and colleagues[31, 43] at MIT was used to solve the EVP.

2.1.2 Importance of the hydrodynamic coefficient database

So far in the EVP formulation, the dependence of the hydrodynamic coefficients C_m and C_{lv} on the frequency ω and amplitude Y of the vibration was assumed known. This in general is not the case and as is evident from Equation 2.10 the relationship between $C_m = f(\omega, Y)$, $C_{lv} = f(\omega, Y)$, ω, and Y, is crucial in determining the solution of the EVP or equivalently in predicting the mode shape and frequency of vibration.

By accepting a "strip theory" approach, one may assume that locally (i.e. for a small section of the flexible body) the relevant nondimensional parameters for the flexible cylinder are the same as those for a rigid cylinder undergoing VIV. For a rigid cylinder dimensional analysis dictates that the relevant nondimensional quantities are:

(1) true reduced frequency f_r, (2) nondimensional amplitude A^*, and (3) Reynolds number (based on diameter) Re_D.

$$f_r = \frac{\omega D}{2\pi U} \tag{2.11}$$

$$A^* = A/D \tag{2.12}$$

$$Re_D = \frac{UD}{\nu} \tag{2.13}$$

where ν is the fluid kinematic viscosity. The dependence of the hydrodynamic coefficients C_m and C_{lv} to the Reynolds number is rather weak (compared to the other two parameters) and may be neglected[15]. Thus a complete hydrodynamic coefficient database may be defined as the mapping between:

$$C_m = f(f_r) \tag{2.14}$$

$$C_{lv} = f(f_r, A^*) \tag{2.15}$$

Equations 2.14 and 2.15 define a full hydrodynamic coefficient database and are extremely important in solving the EVP (i.e. making accurate predictions of the reiser response).

It cannot be overstated how the quality of the acquired hydrodynamic database is key to making VIV predictions by providing accurate estimates of the hydrodynamic forcing (Equation 2.9) to be used when solving the EVP. The hydrodynamic coefficient database essentially serves as a link between the semi-empirical, physics-informed forcing model and reality. Given the strong evidence of the correlation between the vortex dynamics to the added mass and lift coefficients[14, 37, 35], the databases may not only be used to make accurate predictions but also to understand VIV physics and to infer vortex hydrodynamics.

2.2 Learning hydrodynamic coefficient databases from data

We have established a complete forward model which is able to make predictions of riser responses. We now investigate how the forward model may be combined with data (experimental, field, CFD, etc.) so that databases may be machine-learned and used to enhance the predictive accuracy of the forward model or studied to illuminate VIV physics.

2.2.1 Inverse problem definition

So far we have a forward model which given as inputs: (1) the riser geometry and specifications, (2) the incoming stream current profile, (3) a hydrodynamic coefficient database, may be used to predict a riser's response.

Table 2.1: Forward model inputs and outputs

Input	**Output**
Riser geometry and specifications	Amplitude response
Stream current profile	Frequency response
Hydrodynamic database	

Then, provided a set of data in which: (1) the riser geometry, (2) the stream current profile, and (3) the riser response are known, the inverse prediction problem may be defined as the search for the hydrodynamic coefficient database which optimally predicts the data. Schematically this may be shown in Figure 2-2.

The following steps are necessary to proceed from defining the inverse problem to its mathematical formulation: (1) The hydrodynamic coefficient database must be mapped to a set of parameters which completely define it, (2) The parametric hydrodynamic coefficient database must be used with the forward model to make predictions of the (known) responses of the training data set, and (3) the parametric space defining the database must be searched in order to find the set of parameters which makes the optimal predictions according to a relevant objective.

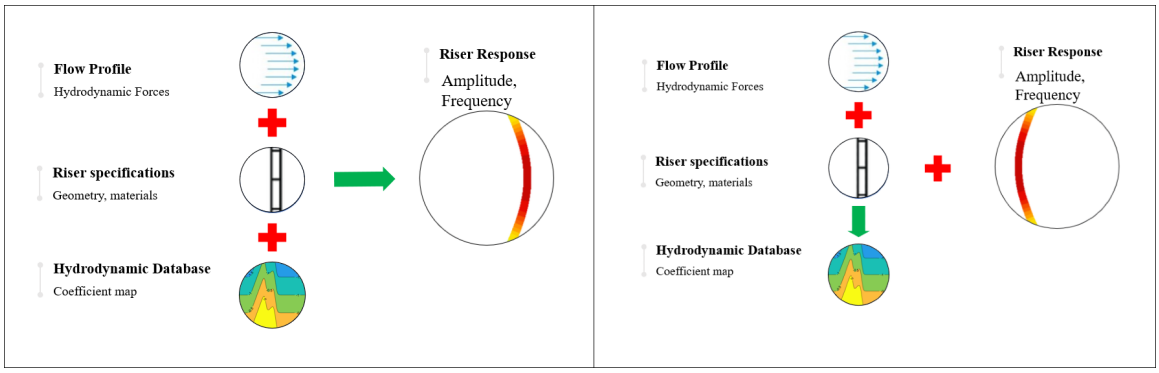

Figure 2-2: Forward model (left) and inverse problem (right)

2.2.2 Hydrodynamic feature extraction (database parametrization)

Prior (empirical) information of the approximate shape of the expected added mass coefficient, $C_m = f(f_r)$ and lift coefficient in phase with velocity, $C_{lv} = f(f_r, A^*)$, was used to formulate a set of hydrodynamic parameters to model Equations 2.14 and 2.15. Specifically, the geometry of the most extensive hydrodynamic coefficient database available, that obtained at MIT by Gopalkrishnan et al. in 1993[15] was used.

The added mass coefficient, C_m is a function of f_r only, making it easy to parametrize as a 2D piece-wise linear curve with parameters defining corner points and then smoothed using a softplus function. This is shown in Figure 2-3.

Parametrizing the lift coefficient in phase with velocity, C_{lv}, which is a function of both f_r and A^* is slightly more complicated. Since the C_{lv} is a surface plot (shown in Figure 2-4), intermediate curves were introduced.

Contours parallel to the A^* axis (i.e. $C_{lv} = f(A^*)$ given f_r constant - an indicative example is shown as a blue solid line in Figure 2-4) were parametrized as two piecewise linear sections. Then to completely define the surface, two additional contours were used. One perpendicular to the A^* axis; the contour of $C_{lv} = f(f_r)$ at $A^* = 0$ (shown as red in Figure 2-4), and another, $A^*_c = f(f_r)$ (shown as purple in Figure 2-4) to govern the transition point of the C_{lv} from increasing to decreasing. The parametric

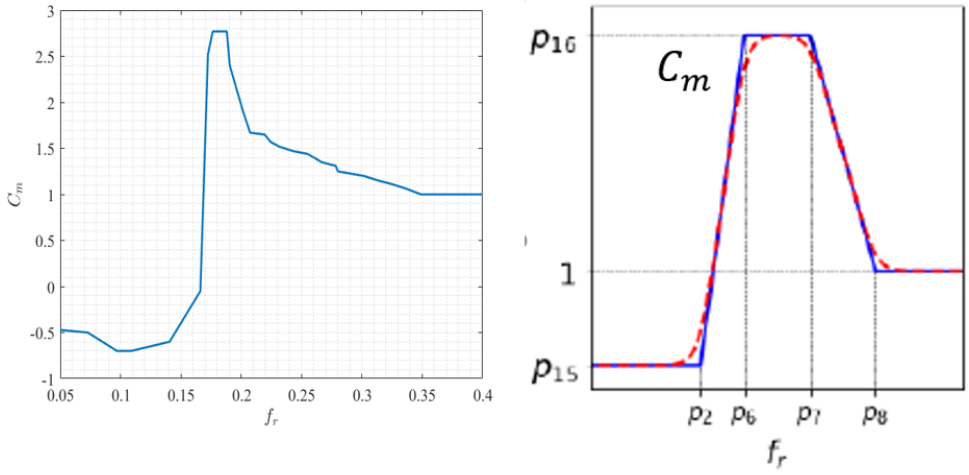

Figure 2-3: Gopalkrishnan C_m (left) and parametric form (right)

forms of these three remaining intermadiate curves are shown in Figure 2-5. The $C_{lv} = f(f_r)$ at $A^* = 0$ intermediate curve as well as the $A_c^* = f(f_r)$ curve were both parametrized as piecewise linear double peak curves. Corner point coordinates were used to define parameters and the shapes were smoothed using a softplus function. The double peak not only approximates the Gopalkrishnan database well in terms of quality but is necessary in order to account for both cross-flow and in-line effects.

Nineteen parameters ($\boldsymbol{p} : p_i,\ i \in [1, 19]$) were selected in total to describe the C_m vs. f_r, $C_{lv,0}$ vs. f_r, A_c^* vs. f_r, and C_{lv} vs. A^* curves which form a complete hydrodynamic coefficient database. The last parameter (p_{19}) was used as the scaling factor of the softplus function.

The mathematical formulation of the parametric (reduced order) model is as follows. Before proceeding to the coefficient formulation, the softplus function is first defined:

$$sf(x, \boldsymbol{p}) = p_{19} \cdot \ln\left(1 + \exp\frac{x}{p_{19}}\right) \tag{2.16}$$

where p_{19} serves as a scaling constant. Then, the C_m curve may be parametrized by Equation 2.17 as follows:

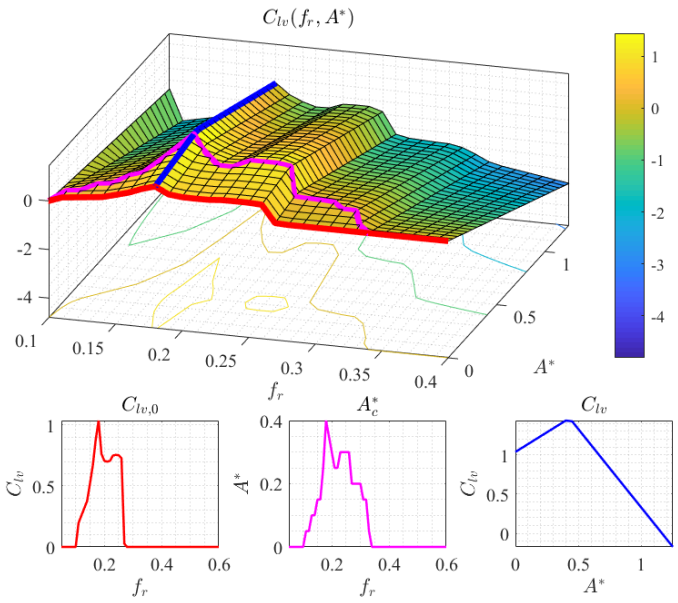

Figure 2-4: Gopalkrishnan $C_{lv} = f(f_r, A^*)$

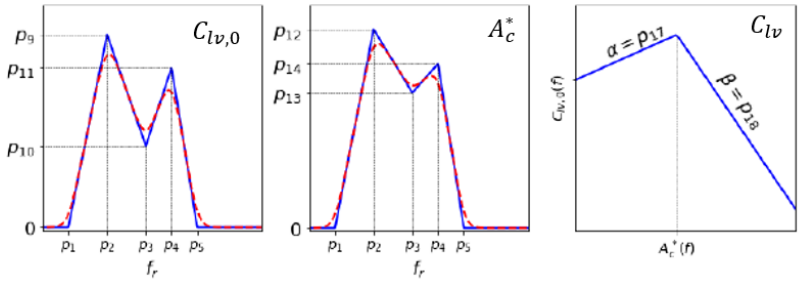

Figure 2-5: Intermediate curve parametrization

$$\hat{C}_m(f_r, \boldsymbol{p}) = p_{15} + \frac{p_{16} - p_{15}}{p_6 - p_2}[sf(f_r - p_2) - sf(f_r - p_6)] + \frac{1 - p_{16}}{p_8 - p_7}[sf(f_r - p_7) - sf(f_r - p_8)] \tag{2.17}$$

where $\hat{C}_m(f_r, \boldsymbol{p})$ is the parametric form of the C_m curve. The $C_{lv,0}$ may be represented parametrically as shown in Equation 2.18.

$$\begin{aligned}\hat{C}_{lv,0}(f_r, \boldsymbol{p}) = &\frac{p_9}{p_2 - p_1}[sf(f_r - p_1) - sf(f_r - p_2)] \\ &+\frac{p_{10} - p_9}{p_3 - p_2}[sf(f_r - p_2) - sf(f_r - p_3)] \\ &+\frac{p_{11} - p_{10}}{p_4 - p_3}[sf(f_r - p_3) - sf(f_r - p_4)] \\ &+\frac{-p_{11}}{p_5 - p_4}[sf(f_r - p_4) - sf(f_r - p_5)]\end{aligned} \tag{2.18}$$

where $\hat{C}_{lv,0}(f_r, \boldsymbol{p})$ is the parametric form of the $C_{lv,0}$ curve. Accordingly, the A_c^* curve may be represented as in Equation 2.19.

$$\begin{aligned}\hat{A}_c^*(f_r, \boldsymbol{p}) = &\frac{p_{12}}{p_2 - p_1}[sf(f_r - p_1) - sf(f_r - p_2)] \\ &+\frac{p_{13} - p_{12}}{p_3 - p_2}[sf(f_r - p_2) - sf(f_r - p_3)] \\ &+\frac{p_{14} - p_{13}}{p_4 - p_3}[sf(f_r - p_3) - sf(f_r - p_4)] \\ &+\frac{-p_{13}}{p_5 - p_4}[sf(f_r - p_4) - sf(f_r - p_5)]\end{aligned} \tag{2.19}$$

where $\hat{A}_c^*(f_r, \boldsymbol{p})$ is the parametric form of the non-dimensional critical amplitude A_c^*. Finally, the value of the lift coefficient, C_{lv} may be calculated according to Equation 2.20.

$$C_{lv}(A^*, \boldsymbol{p}) = \begin{cases} C_{lv,0} + p_{17} \cdot A^* & if A^* \leq A_c^* \\ C_{lv,0} + p_{17} \cdot A_c^* - p_{18} \cdot (A^* - A_c^*) & if A^* > A_c^* \end{cases} \tag{2.20}$$

The values of the parameters were constrained as follows based off empirical knowledge:

Table 2.2: Hydrodynamic feature (parameter) constraints

p_1	$p_2 - p_8$	p_9	$p_{10} - p_{14}$	p_{15}	p_{16}	p_{17}	p_{18}	p_{19}
(0.0, 0.5)	(0,1)	(0,2)	(0,1)	(-1,1)	(1,5)	(0.1-5)	(0.1, 5)	(0,0.005)

It should be noted that the reduced order parametric model allows for shared parameters between the 4 curves defining the complete parametric database. For instance, parameters $p_1 - p_5$ are shared between the $C_{lv,0} = f(f_r)$ and the $A_c^* = f(f_r)$ curves. The complete parametrization may be visualized in Figures 2-3 and 2-5.

2.2.3 Learning problem formulation

Given a complete set of parameters, a database is well defined and may be used with a forward model to make predictions of the riser's response to specific inputs. Given a set of data, the optimal set of parameters in terms of predicting the correct amplitude and frequency of motion may be searched.

In this work, we are interested in making accurate predictions of the amplitude of vibration as a function of span as well as of the frequency of vibration. Then we may formulate the objective function as follows, in order to penalize the amplitude and frequency discrepancy between observation (data) and prediction (forward model):

$$J(\boldsymbol{p}) = \sum_{i=1}^{N_{V_r}} \left[\frac{1}{L} \int_0^L |A_i - \hat{A}_i(\boldsymbol{p})| dx + \lambda |f_i - \hat{f}_i(\boldsymbol{p})| \right] \tag{2.21}$$

where N_{V_r} is the number of velocities tested, A is the observed amplitude, $\hat{A}(\boldsymbol{p})$ is the predicted amplitude using the parametric database, f is the vibration frequency, and $\hat{f}(\boldsymbol{p})$ is the predicted vibration frequency. The integral expression for the amplitude ensures that the discrepancy between the observed amplitude and the predicted one is minimized across the whole riser span, L.

In order to ensure that the geometry of the optimal parametric database for a given data set does retains some features of its initialized parametric form, additional regularization terms are added. The regularization terms were obtained through trial and error and helped improve the results obtained using Equation 2.21. Specifically, the distance between parameters $(p_5 - p_1)$ compared to 0.1 (both) squared was penalised using a factor of β and so was the magnitude of the scaling factor of the softplus function, p_{19} using a factor of γ. The exact regularization terms are shown in Equation 2.22.

$$R(\boldsymbol{p}) = \beta \left[\frac{p_5 - p_1}{0.1} \right]^2 + \gamma |p_{19}| \tag{2.22}$$

where the factors β and γ are chosen arbitrarily. Provided we only have discrete reconstructed amplitude points across the riser's span, we can numerically approximate the integral expression in Equation 2.21 as:

$$\frac{1}{L} \int_0^L |A_i - \hat{A}_i(\boldsymbol{p})| dx \approx \frac{1}{L} \sum_{n=1}^{N_L} \sqrt{\left[A_{i,n} - \hat{A}_{i,n}(\boldsymbol{p}) \right]^2} \cdot \Delta x_n \tag{2.23}$$

Further normalizing the amplitude by the cylinder's diameter and averaging we can replace the term shown in Equation 2.23 with the (slightly different) root mean square error of the nondimensional amplitude across the whole span. The final form is advantageous in controlling the balancing factors λ, β, and γ and does not alter the fundamental nature of the Equation 2.21. The learning problem may then be characterised by the following objective function:

$$J(\boldsymbol{p}) = \sum_{i=1}^{N_{V_r}} \left[\lambda \sqrt{\frac{1}{N_L} \sum_{n=1}^{N_L} [A^*_{i,n} - \hat{A}^*_{i,n}(\boldsymbol{p})]^2} + \sqrt{[f_i - \hat{f}_i(\boldsymbol{p})]^2} \right] + \beta \left[\frac{p_5 - p_1}{0.1} \right]^2 + \gamma |p_{19}| \tag{2.24}$$

where N_L is the number of points used across the span. Minimizing Equation 2.24 is equivalent to finding the parametric hydrodynamic coefficient database which optimally predicts the given training data set.

Obtaining riser amplitude (displacement) data is an expensive process which requires making assumptions and further processing raw measured quantities (usually strain and acceleration). Since strain data are readily available from experiments or the field and in practice are much easier to obtain, it was deemed appropriate to demonstrate that the methodology can also be successful using strain data to learn hydrodynamic coefficients. In this case the objective function assumes the following form.

$$J(\boldsymbol{p}) = \sum_{i=1}^{N_{Vr}} \left[\lambda \sqrt{\frac{1}{N_L} \sum_{n=1}^{N_L} [\epsilon_{i,n} - \hat{\epsilon}_{i,n}(\boldsymbol{p})]^2} + \sqrt{[f_i - \hat{f}_i(\boldsymbol{p})]^2} \right] + \beta \left[\frac{p_5 - p_1}{0.1} \right]^2 + \gamma |p_{19}| \tag{2.25}$$

where ϵ is the observed strain directly measured on the body and $\hat{\epsilon}(\boldsymbol{p})$ is the predicted strain using the parametric database and the forward model.

2.2.4 Optimization routine

Optimizing the objective function (Equation 2.24 or Equation 2.25) is highly nontrivial since the optimization problem at hand is non-convex, non-smooth, and spans a 19-dimensional space. Gradient methods were ruled out mainly because of two reasons: 1. obtaining a gradient estimate requires 19 evaluations of the forward model using finite differences (very expensive computationally) and 2. the geometry of the space defined by fixing all parameters but one in many cases resembles a "staircase" making the gradient either very large, or almost zero.

A stochastic coordinate descent method was selected since it seemed to work best with the problem. A schematic of the optimization update is shown in Figure 2-6. Given an estimate of the hydrodynamic database, the forward model is evaluated and the prediction is then compared with the observed response in the data set. Based off the discrepancy between observation and prediction, the estimate is perturbed to better predict the data.

The stochastic coordinate descent algorithm may be described as follows for the given problem. Provided a set of parameters $\boldsymbol{p}$ such that:

$$\boldsymbol{p} = (p_1,\ p_2,\ p_3, ...,\ p_{18},\ p_{19}) \tag{2.26}$$

we iterate along each direction (defined by coordinate p_i), one at a time, and at direction i solve the one-dimensional problem defined by Equation 2.27.

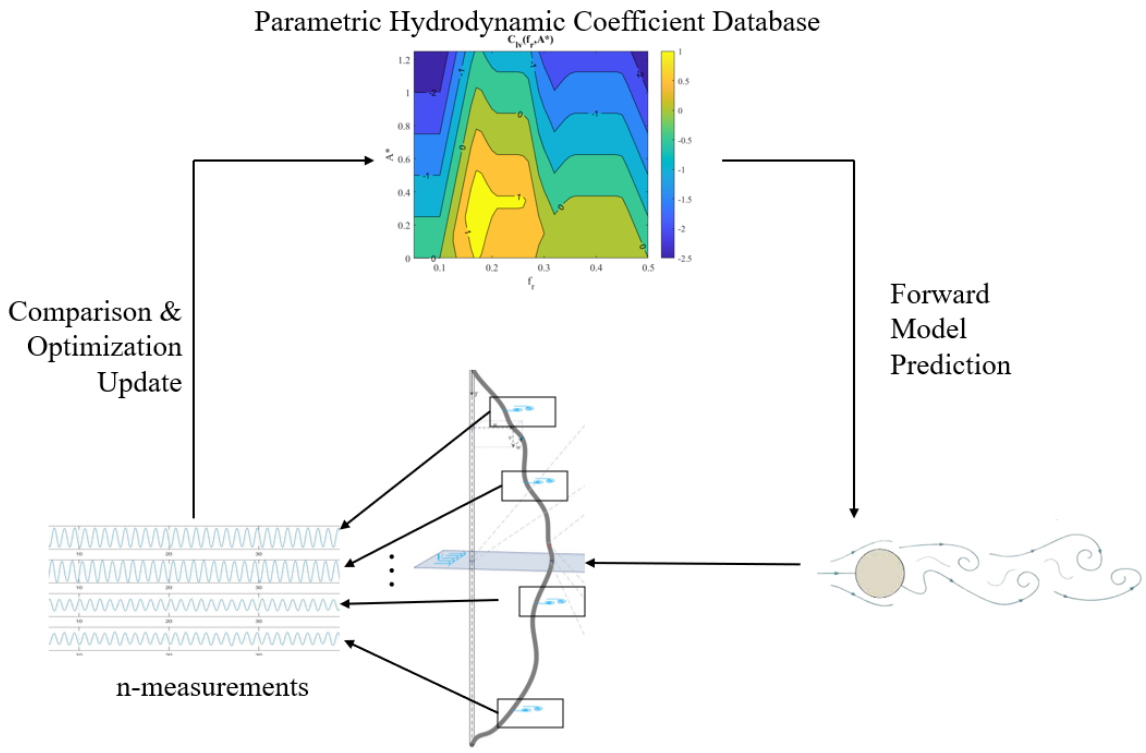

Figure 2-6: Optimization update

$$p_i = \arg\min_{z} \; J(p_1,\; p_2,\; p_3, ...,\; p_{i-1},\; z,\; p_{i+1}, ...,\; p_{18},\; p_{19}) \tag{2.27}$$

Equation 2.27 may be solved using a line search algorithm or ideally using a closed form expression. In our case, the "staircase" nature of the line search problem obtained after isolating directions from Equation 2.24 made the algorithm slow and poorly performing.

More rapid convergence was achieved by using the alternative approach of evaluating the objective function at a perturbation of the given estimate along a fixed direction, specified either as the direction of a specific parameter p_i or a random direction; an approach similar to a random search algorithm. Specifically, an iterative scheme of the following form was employed.

$$\boldsymbol{p}^* = \boldsymbol{p} + \delta_i \boldsymbol{v_i} \tag{2.28}$$

where $\boldsymbol{p}^*$ is the trial (perturbed) value of the parameters defining the hydrodynamic coefficient database and

$$\delta_i = \underset{\delta \in \Delta}{\arg\min} \; J(\boldsymbol{p} + \delta \boldsymbol{v_i}) \tag{2.29}$$

where $\Delta = \{0, \delta_1, \delta_2, ..., \delta_{n_s}\}$, a set including 0 and n_s samples of some distribution p_δ, in this case a normal distribution (with geometrically decaying variance after a set number of iterations). The direction $\boldsymbol{v_i}$ was specified as either a column vector chosen from the identity matrix with randomly permuted columns or a random unitary matrix. In such a way the perturbation directions were not constrained to lie only along the direction of the parameters. In order to enforce open boundaries for the optimization problem, the algorithm was performed on the transformed set of variables $\boldsymbol{q}$. The transformation from p_i to q_i was performed according to Equation 2.30.

$$q_i = \sigma^{-1}\left(\frac{p_i - p_{i,min}}{p_{i,max} - p_{i,min}}\right) \tag{2.30}$$

where σ is the sigmoid function, mapping $\mathbb{R}$ to $(0, 1)$, and $p_{i,min}$ & $p_{i,max}$ are the minimum and maximum allowed values of each parameter p_i according to Table 2.2. The pseudocode for the optimization routine is shown below.

Stochastic Coordinate Descent Algorithm $(\boldsymbol{J}, \boldsymbol{p}_0)$

1. Initialize $\boldsymbol{q} = \boldsymbol{q}_0 = \boldsymbol{q}(\boldsymbol{p_0})$
2. **for** $i = 1, 2, ..., n$ **do:**
3. Select $\boldsymbol{V} \in \mathbb{R}^{\,d \times d} : \boldsymbol{V^T V} = \boldsymbol{I}_{d \times d}$
4. **for** $j = 1, 2, ..., d$ **do:**
5. $\Delta = \{0, \delta\}_{k=1}^{n_s+1} : \delta_k \sim p_\delta^{(i)}$
6. $k_{best} = \arg\min_k J(\boldsymbol{p}(\boldsymbol{q} + \delta_k \ \boldsymbol{v}_j))$
7. **if** $J(\boldsymbol{p}(\boldsymbol{q} + \delta_{k_{best}} \boldsymbol{v}_j)) < J(\boldsymbol{p}(\boldsymbol{q}))$ **then**:
8. $\boldsymbol{q} = \boldsymbol{q} + \delta_{k_{best}} \boldsymbol{v}_j$
9. return $\boldsymbol{p} = \boldsymbol{p}(\boldsymbol{q})$

Chapter 3

Results

The goal of the learning problem was to determine the optimal set of parameters, i.e. to determine the optimal parametric hydrodynamic coefficient database, in order to make predictions of riser's vortex induced cross-flow vibration responses given a set of riser response data. In order to assess the success of the learning problem on the various training data sets, the riser temporal-mean amplitude across the whole span, as well as the vibration frequency predicted using the optimal parametric hydrodynamic databases were compared with the observed responses.

3.1 Initial condition

Defining a suitable initial condition for the learning problem was deemed appropriate since initializing at random would, in the least, slow down the convergence of the optimization algorithm, and possibly be partly carried down to the converged result in regions with not many training data. The physics-informed nominal VIVA[31, 43] database (that of Gopalkrishnan et al.[15]) which has been obtained via rigid cylinder forced vibrations was selected as the appropriate initial condition.

In order to determine the set of initial parameters $\boldsymbol{p_0}$ which optimally parametrize the Gopalkrishnan[15] database, an optimization problem was formulated to minimize the discrepancy between the $C_{lv} = f(f_r, A^*)$ and $C_m = f(f_r)$ of the Gopalkrishnan database and the initial parametric database defined by $\hat{C}_{lv} = f(f_r, A^*, \boldsymbol{p_0}), \hat{C}_m =$

$f(f_r, \boldsymbol{p_0})$. The objective function to be minimized in this context is as follows:

$$J(\boldsymbol{p}) = \int_{A^*_{min}}^{A^*_{max}} \int_{f_{r_{min}}}^{f_{rmax}} |C_{lv}(f_r, A^*) - \hat{C}_{lv}(f_r, A^*, \boldsymbol{p})| \; df_r \; dA^* + \\ + \lambda \int_{f_{r_{min}}}^{f_{rmax}} |C_m(f_r) - \hat{C}_m(f_r, \boldsymbol{p})| \; df_r \tag{3.1}$$

where λ is a balancing factor chosen arbitrarily. Then the best possible approximation of the Gopalkrishnan database by the parametric reduced order model would be:

$$\boldsymbol{p_0} = \arg\min_{\boldsymbol{p}} J(\boldsymbol{p}) \tag{3.2}$$

with $J(\boldsymbol{p})$ as defined by Equation 3.1. The integral expressions in Equation 3.1 may be discretized and scaled without altering the nature of the expression. Specifically, a discrete equivalent optimization expression is given in Equation 3.3.

$$J(\boldsymbol{p}) = \sum_{i=1}^{N_{A^*}} \sum_{j=1}^{N_{f_r}} \frac{\sqrt{(C_{lv}(f_{r_j}, A^*_i) - \hat{C}_{lv}(f_{r_j}, A^*_i, \boldsymbol{p}))^2}}{N_{f_r} \cdot N_{A^*}} + \lambda \sum_{j=1}^{N_{f_r}} \frac{\sqrt{(C_m(f_{r_j}) - \hat{C}_m(f_{r_j}, \boldsymbol{p}))^2}}{N_{f_r}} \tag{3.3}$$

where N_{f_r} and N_{A^*} are the number of reduced frequencies and number of non-dimensional amplitudes used, respectively. Provided that the choice of parametrization uses shared parameters between the $\hat{C}_m = f(f_r)$ and $\hat{C}_{lv} = f(f_r, A^*)$ curves, it was deemed appropriate to match either the $\hat{C}_m = f(f_r)$ curve or the $\hat{C}_{lv} = f(f_r, A^*)$ for the initial condition. Given the greater complexity of the latter curve, it was decided that the $\hat{C}_{lv} = f(f_r, A^*)$ curve should be matched (i.e. $\lambda = 0$ in Equation 3.3) and the evaluation of the lift coefficient of the Gopalkrishnan database would be interpolated at the centers of the grid points. A regularization term penalizing the magnitude of the scaling factor of the softplus function (p_{19}) was added and the final objective expression was:

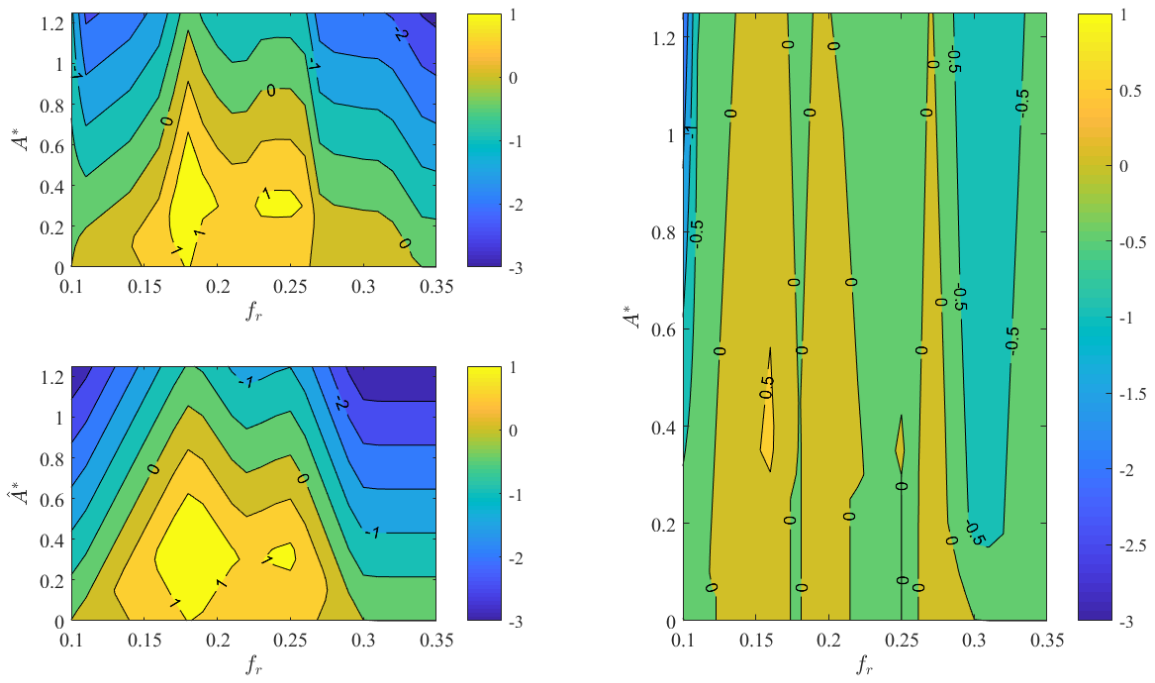

Figure 3-1: Initial condition: C_{lv} contour of Gopalkrishnan database (top left) and $\hat{C}_{lv}$ contour of initialized parametric database (bottom left). The difference $\hat{C}_{lv} - C_{lv}$ is plotted on the right

$$J(\boldsymbol{p}) = \sum_{i=1}^{N_{A^*}-1} \sum_{j=1}^{N_{fr}-1} \frac{\sqrt{\left[C_{lv}(\frac{f_{r_j}+f_{r_{j+1}}}{2}, \frac{A_i^*+A_{i+1}^*}{2}) - \hat{C}_{lv}(\frac{f_{r_j}+f_{r_{j+1}}}{2}, \frac{A_i^*+A_{i+1}^*}{2}, \boldsymbol{p})\right]^2}}{N_{f_r} \cdot N_{A^*}} + \beta|p_{19}|, \tag{3.4}$$

where the value of the balancing factor β was chosen arbitrarily. The resulting C_{lv} contour as well as the training contour are shown in Figure 3-1.

The optimization was performed accross the range of $f_r = [0.1, 0.3]$ and $A^* = [0, 1.2]$, where most observed VIV responses occur. The reduced order parametric result qualitatively agrees with the training database both in terms of magnitude and contour shape in that region. The nineteen (double peak) parametrization offers flexibility in terms of capturing the two "peak" contours of the training database in that region as is evident in Figure 3-1.

For low f_r, close to 0.1 the behavior the Gopalkrishnan contours is not well ap-

proximated, as the model is unable to capture the sharp corners of the training set. In addition there is a small region defined by $f_r \approx 0.15$ and $A^* \approx [0.4 - 0.6]$ where the parametric initial condition overestimates the Gopalkrishnan database C_{lv} by about 0.5. Discrepancy is also observed for $f_r > 0.3$, especially for the negative valued contours (outside the optimization range). Given that VIV occurs at a range of approximately $f_r \in [0.15, 0.30]$ where the parametrization matches the training data closely, the parametric model and initial condition were deemed adequate, especially since further refinement of the database would follow during the training stage of the learning problem.

3.2 Uniform flexible riser in uniform flow

The first application of the methodology included reproducing the results by Rudy et al.[27] with the optimal initial condition. Training was done on the scaled (bare cylindrical) riser experiments conducted as part of the Norwegian Deep Water Programme (NDP)[7]. The riser specifications are shown in Table A.1. The flow was uniform and the stream velocity was varied from 0.3 m/s to 2.4 m/s in 0.1 m/s increments. The test numbers and corresponding flow velocities are shown in Table A.2. The tested Reynolds numbers lied in the range $Re_D \approx 7.1 \cdot 10^3 - 5.7 \cdot 10^4$.

3.2.1 Displacement training

Initially, training was done using N=900 points of the reconstructed displacement uniformly spaced across the riser's span. The objective for the learning problem was Equation 2.24.

The amplitude responses as a function of the span are shown in Figure 3-2. The Figure includes various plots of the mean riser amplitude response (nondimensionalized by the diameter) as a function of span (nondimensionalized by the riser length). The amplitude is plotted on the y-axis while the spanwise position is plotted on the x-axis. The observed (experimental) response is plotted as a solid blue line while the prediction of the optimal parametric hydrodynamic database is plotted as a solid

black line. Each different subplot corresponds to a different flow velocity as outlined in Table A.2 (flow velocity increases from top left to bottom right).

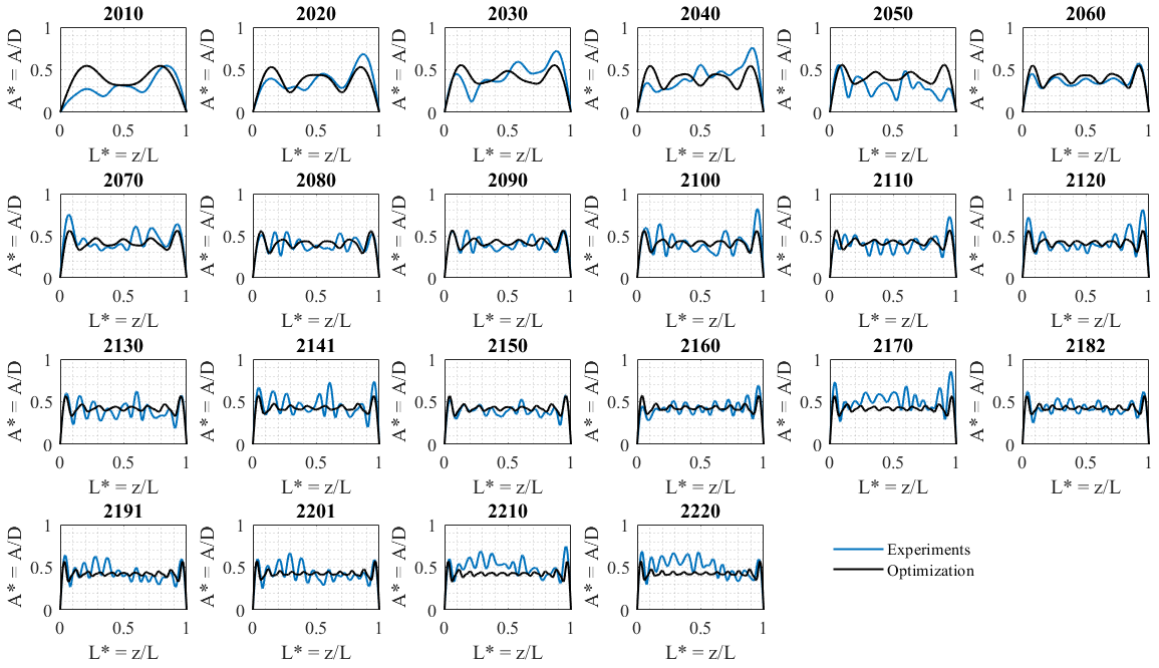

Figure 3-2: NDP uniform amplitude prediction

As Figure 3-2 illustrates there is good agreement between the observed riser amplitude and the predicted one using the optimal parametric hydrodynamic database after training on the data set. On average, the amplitude prediction of the trained forward model matches observation with errors of less than 10-15%. The high mode number ($\approx O(10)$) is also predicted although the exact mode number might not have been correctly predicted in every case.

It should be noted that for very low flow velocities, the observed response from the experiments is very asymmetric; in theory we expect a completely symmetric response since this is a symmetric problem. Imperfections in the setup/procedure excite an asymmetrical response which is beyond the predicting capabilities of our model. Given that there is no preferred direction on the riser as well, the asymmetry most likely is initiating by geometric imperfections in the setup and propagates towards a "random" direction. For higher flow velocities however experimental imperfections become a lot

less significant and the response observed is a lot more symmetric.

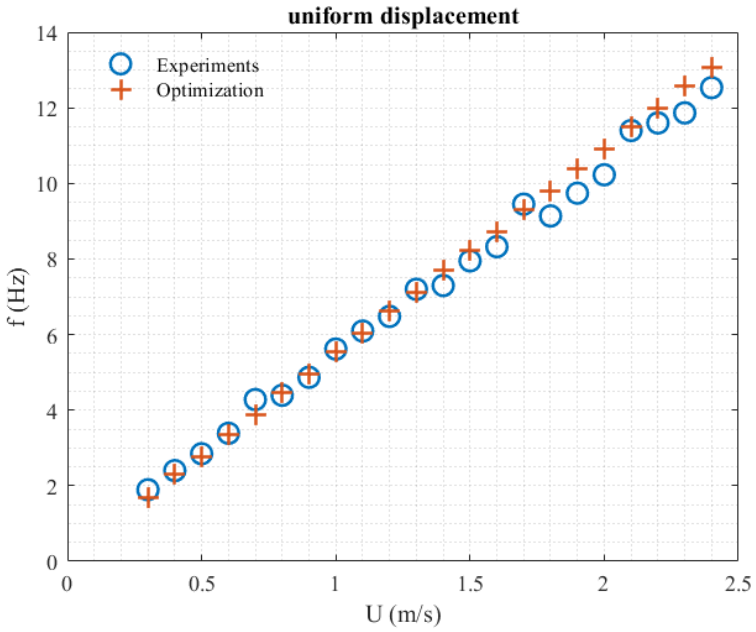

Figure 3-3: NDP uniform frequency prediction

The riser frequency responses are plotted in Figure 3-3. The response frequency is plotted on the y-axis while the stream velocity is plotted on the x-axis. The observed response (experimental) is plotted as a blue circle while the prediction using the extracted database is plotted as an orange plus sign. As is evident, the frequency is very well predicted using the extracted hydrodynamic database with errors of less than 10% and a correct prediction of the trend as well. The success of the uniform riser in uniform flow predictions using displacement data for training serves as a proof of concept for the proposed methodology.

3.2.2 Strain training using sparse sensing

As discussed in Chapter 2, strain measurements are raw data readily available from experiments or field data. However, the number of strain gauges (sensors) is limited and usually (especially in the field) strain sensing is notoriously sparse. By sparse, in this context it is meant that direct strain measurements were made at N=24 uniformly spaced points along the span, compared to the N=900 (reconstructed) displacement

points available along the span; the difference is of one order of magnitude. Additionally, no computational complexity is added when using (raw) strain data compared to displacement data which need to be reconstructed from accelerometer or strain gauge measurements. Although training was done using **direct strain measurements** (and according to Equation 2.25), the quality of the extracted database was measured by comparing the predicted displacement of the riser as well as the frequency response. The results obtained comparing the observed and predicted amplitude response of the riser using the strain trained database are shown in Figure 3-4.

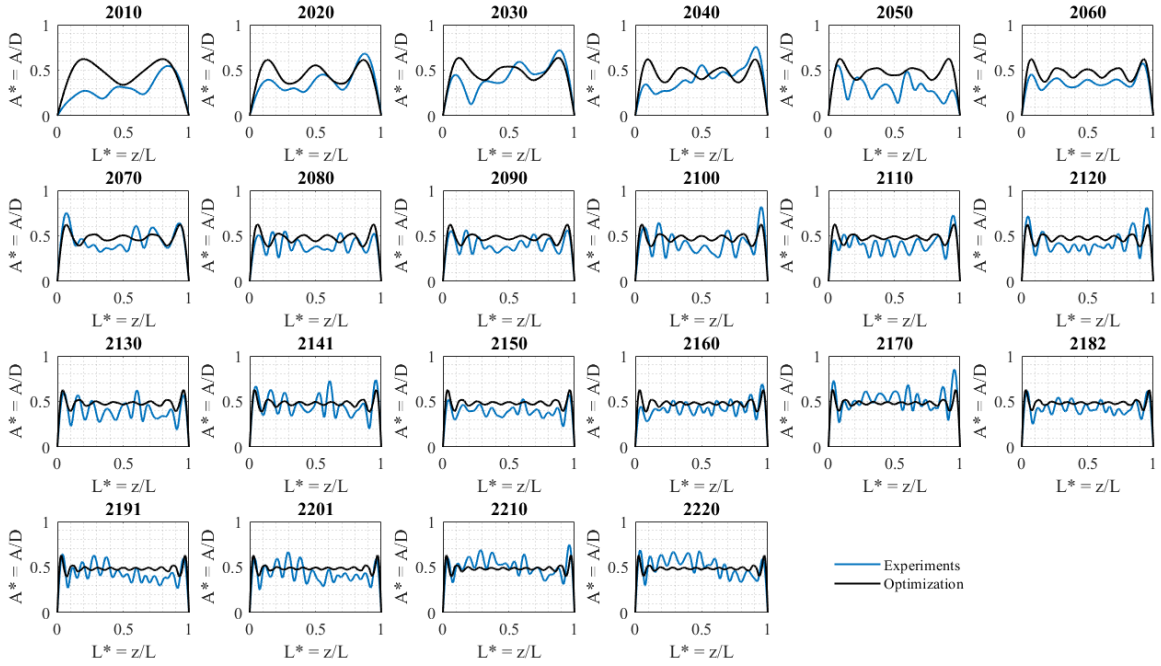

Figure 3-4: NDP uniform amplitude prediction *using strain*

As Figure 3-4 illustrates, there is good agreement between the observed and predicted amplitude using the strain trained database; the high mode number is also predicted. The average error across the span is less than 20%; however, in some cases, the predictions underestimate the variation of the amplitude around midspan. As was the case with the displacement training, for low flow velocities the observed asymmetrical response is not very well predicted, as expected since it is beyond the model's capabilities. For higher flow velocities however the predictions remain accurate although perhaps slightly overestimating the response on average. The obtained

frequency results using the strain trained database are shown in Figure 3-5.

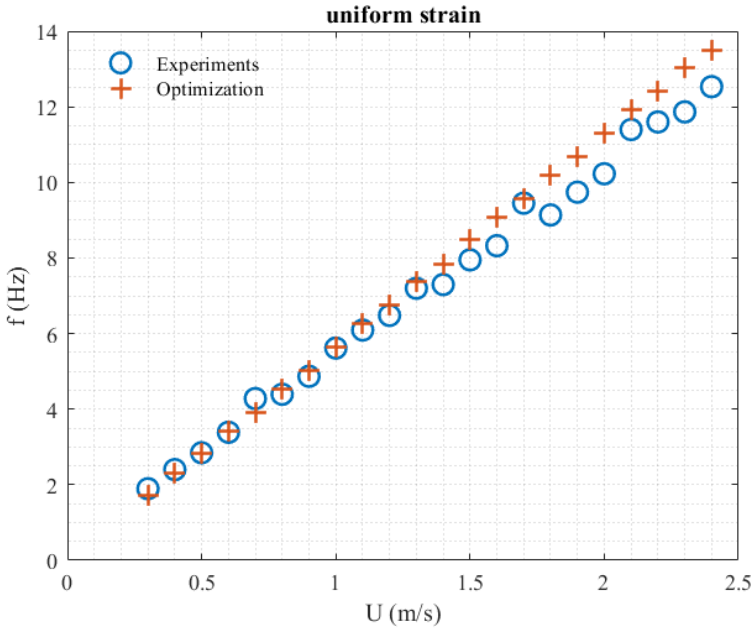

Figure 3-5: NDP uniform frequency prediction *using strain*

As is evident in Figure 3-5, the frequency of vibration is well predicted as a function of the incoming stream velocity and the linear increasing trend is captured. For high flow velocities (i.e. about 2 m/s or higher) the predictions become gradually worse than those for low flow velocities with a maximum error of about 15%.

The prediction results using the extracted database using direct sparse strain measurements demonstrates how databases need not be learned from displacement data which are rather expensive to obtain but may be determined directly from sparse strain measurements along the structure which are in practice easier to obtain.

3.2.3 Displacement vs. strain training

The learning problem was formulated using data from the NDP experiments for a straight uniform riser in uniform flow. Two different optimizations were performed on the same set of experimental data, one displacement based, and the second strain based; in both cases, reconstructed amplitude was compared to predicted amplitude

and so was frequency. It should be noted that N=900 data points across the riser's span were used for training with displacement data whereas N=24 data points across the riser's span were used for training using strain data.

In order to determine the accuracy of the inferred databases the displacement prediction as well as the frequency prediction was compared with the reconstructed displacement from experiments as well as the measured frequency for all tested velocities.

In both training cases, there is agreement between experimental observation and forward model prediction. The results also remain consistent regardless of the training scheme used. A useful measure of comparison would be plotting the time-space averaged amplitude across the riser's span against the stream velocity as predicted by the two extracted databases as well as the predicted frequency as a function of the stream velocity. This is shown in Figure 3-6; the figure also includes the predictions of the forward model using the Gopalkrishnan[15] database which was also used as the initial condition for the learning problem.

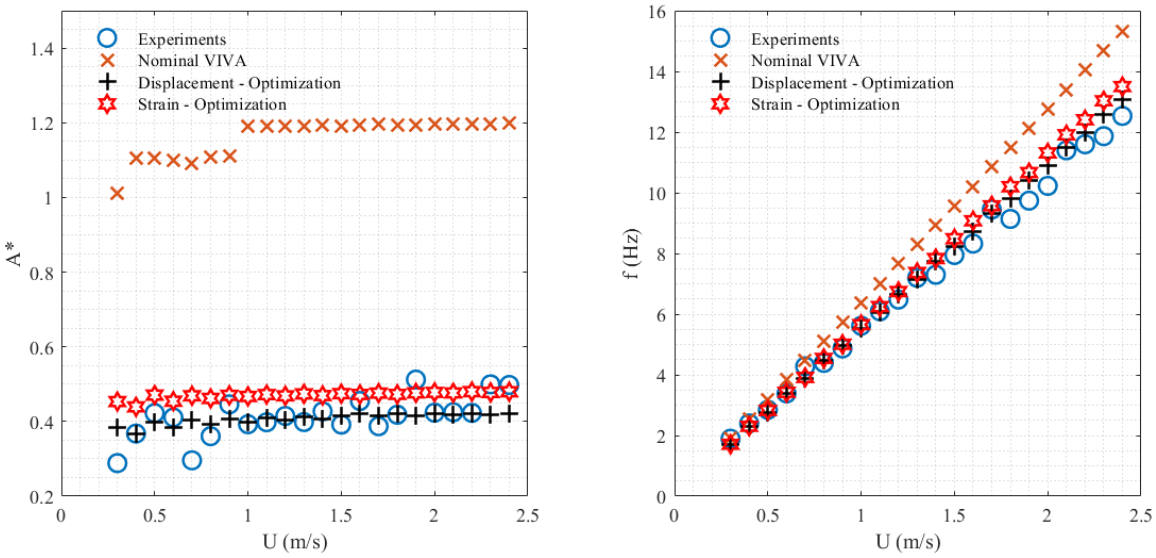

Figure 3-6: Prediction comparison between displacement training, strain training, and Gopalkrishnan.

Figure 3-6 reveals that both the amplitude and the frequency are better pre-

dicted after optimizing the hydrodynamic coefficient database and results are consistent regardless of optimization method. In addition, the figure illustrates how the predictions deviate significantly from those made using the initial condition (i.e. Gopalkrishnan[15]), which means that the databases were refined and make better predictions after training. It should be noted that the displacement trained database makes predictions slightly superior to those of the strain trained database although the difference is small (about 15% at most). Further, this serves to show how the extracted hydrodynamic databases make better predictions than those using the Gopalkrishnan database which was obtained via the traditional rigid cylinder forced vibration experiment method.

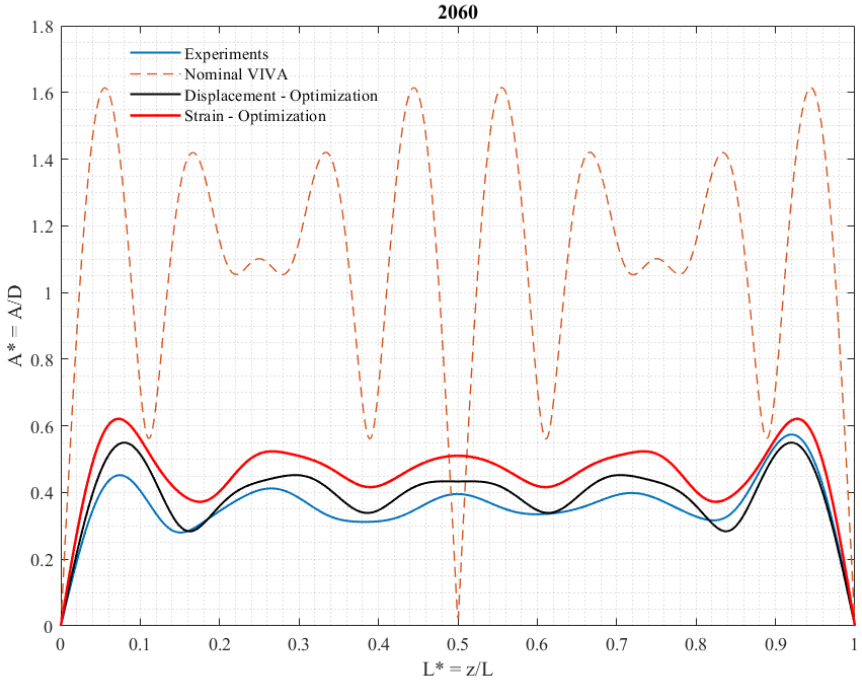

Figure 3-7: Second prediction comparison between displacement training, strain training, and Gopalkrishnan.

As is evident in Figure 3-7, the optimized hydrodynamic database, regardless of optimization method (be that displacement or strain) significantly improves the predictive power of the forward model compared to that of using the Gopalkrishnan database. Not only is the amplitude magnitude prediction more accurate but also

the mode number of the structural response is corrected (at least to some extent), revealing that information regarding the physics which the model was agnostic to prior to the optimization was learned during training. It should be noted that the case presented in Figure 3-7 was chosen because it is one in which the mode number is easily identifiable and also very well predicted by the model.

In terms of computational complexity, the strain based method is advantageous in the sense that displacement training requires reconstructing the displacement which is computationally expensive. In terms of training wall time, both models are similar requiring about 12 hours to train on the given database ($O(10GB)$).

3.3 Uniform flexible riser in stepped uniform flow

In this section, data from Chaplin et al, 2005[8] were used. A straight uniform flexible riser was placed in a stepped incoming stream. The experimental layout is shown in Figure B-1. The particulars of the riser are shown in Table A.3.

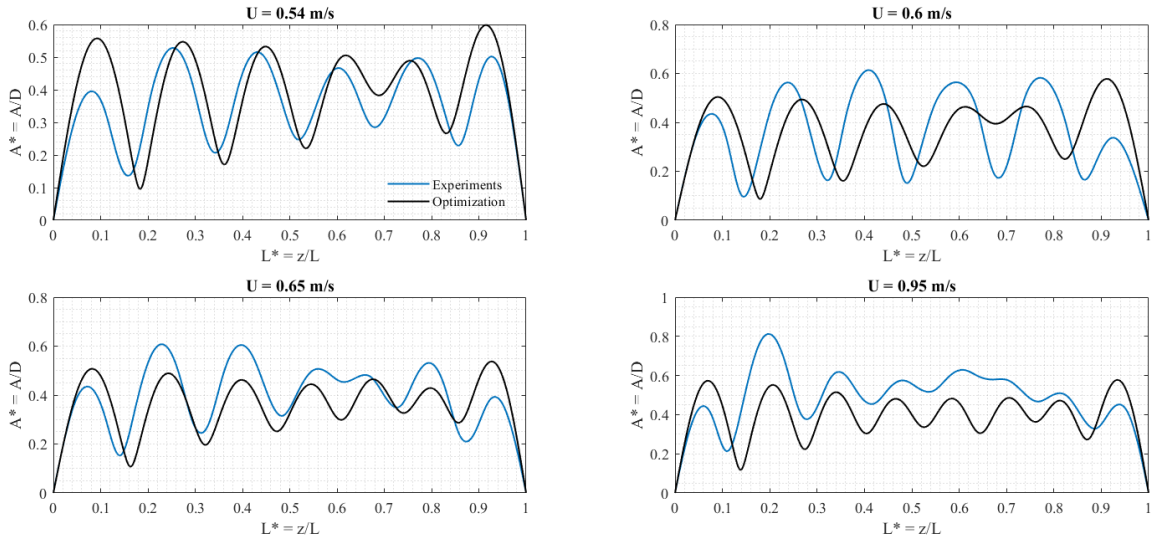

Figure 3-8: Amplitude prediction for uniform riser in stepped current

The velocities tested were $U = 0.54$ m/s, $U = 0.60$ m/s, $U = 0.65$ m/s, and $U = 0.95$ m/s, respectively where only the bottom half of the riser was exposed to

the current while the top half was submerged in still water.

Given the lower $L/D \approx 450$ ratio of this set of experiments compared to the NDP experiments ($L/D \approx 1500$), a lower mode number was expected (and observed) experimentally; the maximum mode number was 8. Training on this data set was done using reconstructed displacement data and according to Equation 2.24.

The amplitude responses after training on the four tested velocities are shown in Figure 3-8. As the figure reveals, the forward model using the extracted hydrodynamic coefficient database makes good predictions of the amplitude, with average erros of less than 10% and both amplitude variations and mode shapes captured. Additionally, prediction of the mode number (i.e. 6, 6, 7, and 8) was correct in all cases with the locations of the peaks to within 10-15% of their true locations.

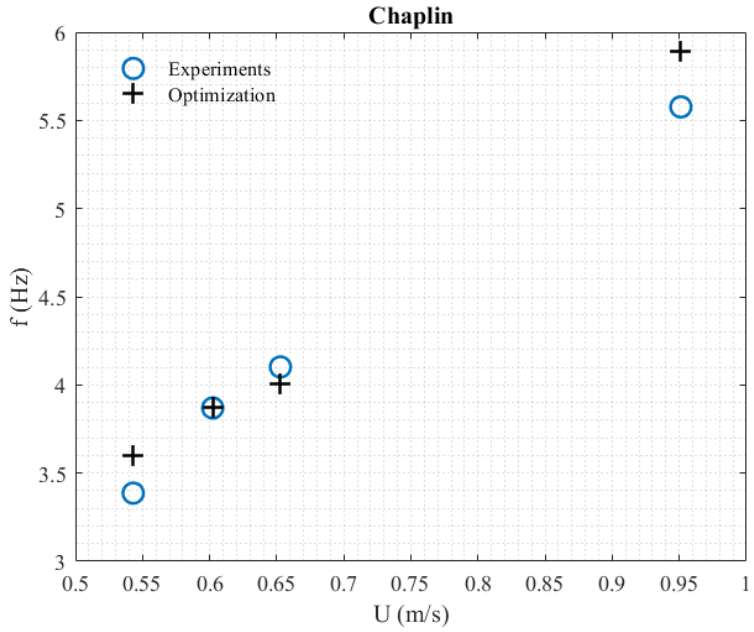

Figure 3-9: Frequency prediction for uniform riser in stepped current

Figure 3-9 shows the frequency predictions using the extracted database. As is evident in the figure, the trained forward model can make frequency predictions with errors of less that 10%.

3.4 Uniform flexible riser in sheared flow

Provided that the ocean currents are non-uniform and usually better approximated by a shear or exponential profile, the methodology was applied to linear triangular shear data provided by the NDP experiments[7]. The same riser model as in the uniform flow cases was used with particulars specified in Table A.1. The test numbers and associated flow velocities are specified in Table A.4.

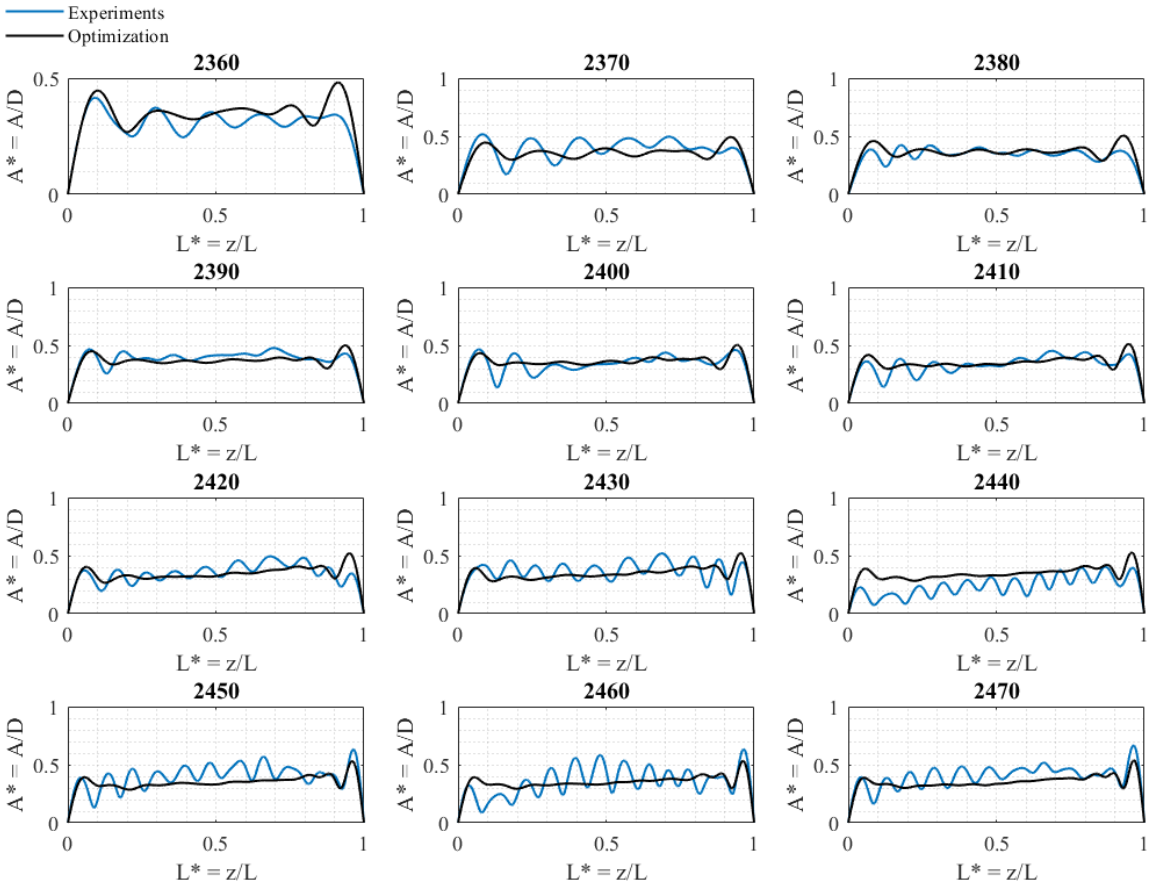

Figure 3-10: Shear flow amplitude prediction

Linear shear introduces non-uniformity of the flow as seen by the structure and accordingly the expected amplitude of vibration across the span is no longer expected to be symmetric. The hydrodynamic coefficient database for the shear flow case was extracted using displacement data and the results for the amplitude response of the flexible cylinders are shown in Figure 3-10.

As Figure 3-10 reveals, the learned database was able to predict the response to good accuracy across the whole span, and in addition capture the expected non-symmetrical response of the flexible structure across the full range of velocities tested. Although on a spanwise average basis responses are predicted with errors of less than 20%, the variation of the amplitude response prediction could be improved as the "wavy" shape of the observed responses is predicted more linear using the trained forward model. Perhaps the addition of a regularization term in the objective penalizing the variation of the response could improve that result.

As far as the frequency response is concerned, good agreement is evident between observed and predicted frequencies for the shear flow cases as is shown in Figure 3-11 with errors of less than 15%.

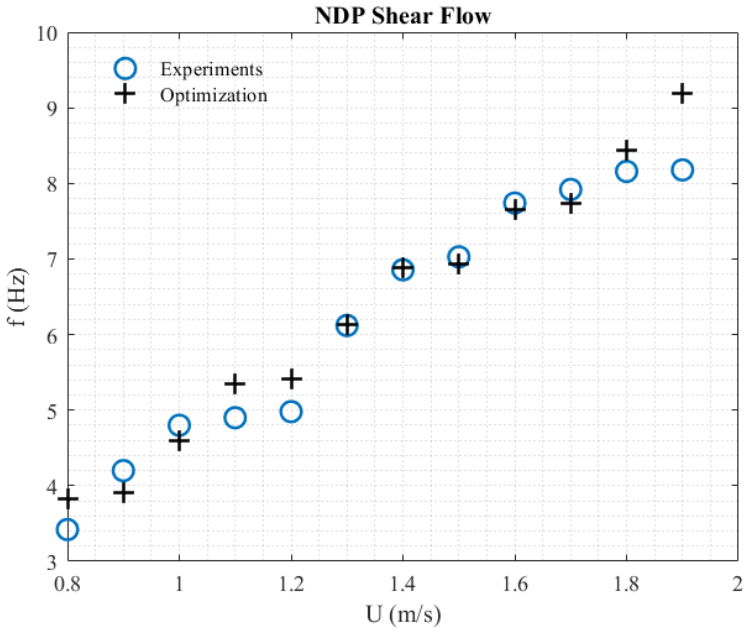

Figure 3-11: Shear flow frequency prediction

Another result obtained from the analysis of the shear flow data is the predicted C_{lv} for the riser as a function of its span as shown in Figure 3-12. In Figure 3-12, the C_{lv} is plotted as a blue solid line with the C_{lv} value plotted on the x-axis while the y-axis shows the location along the structure.

The C_{lv} as a function of the span seems to "switch" sign from positive to negative,

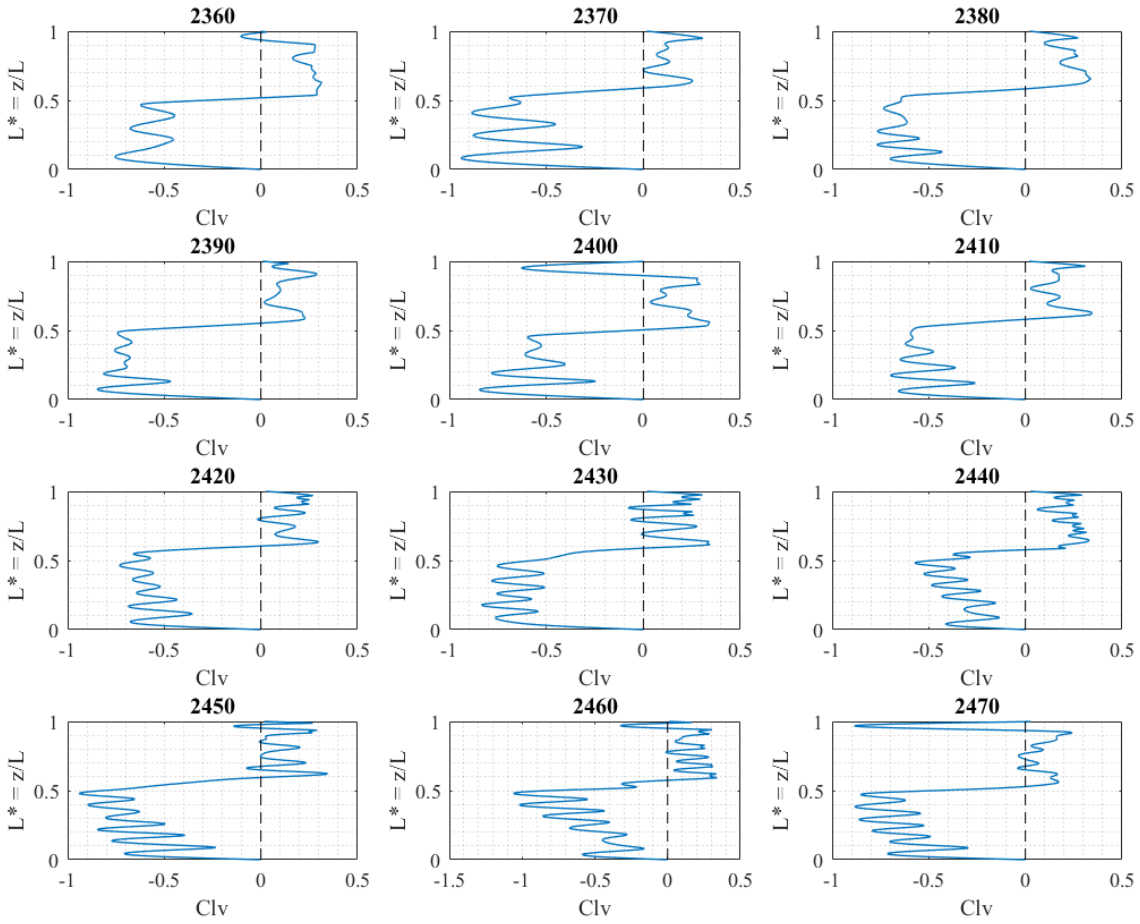

Figure 3-12: Shear flow C_{lv} as a function of span

consistently at approximately mid-span of the riser. This provides insight in the physics of the problem suggesting that about half the riser is absorbing energy from the flow initiating the vibrations while the other half is dissipating energy back into the fluid. This is a well understood result reproduced repeatedly for sheared flow experiments. It may be explained as follows: the structure's half which sees the high amplitude flow velocity gets excited and initiates the vibrations, a travelling wave response is induced with waves travelling from the high velocity region to the low velocity region. At the low velocity region, the travelling wave response is dampened, transferring some energy back to the fluid. This result is of notable importance to show how the proposed methodology need not only be used to make VIV response predictions but may also be used to explain the underlying physics of VIV.

3.5 Catenary flexible riser in uniform flow

Predicting the response of non straight risers is significantly more challenging since the hydrodynamics of the problem change as a function of the structure's span and the structural non-uniformity, i.e. geometric curvature, needs to be considered. Notably, the tension along the structure varies as well and so does the incidence angle of the incoming flow along the span. Finally, allowing the catenary plane to be at an angle with respect to the incoming flow introduces balooning effects which increase the complexity.

Figure B-2 illustrates the experimental setup for the catenary riser experiments. The incoming uniform flow is shown as blue arrows while 4 catenary risers are plotted (in colors: green, purple, mustard, and orange) at four different angles between the catenary plane and the incoming flow which is always parallel to the x-axis as shown in Figure B-2.

The data used for applying the methodology came from the NDP experiments[7] with a scaled catenary riser whose particulars are detailed in Table A.5. Test numbers and corresponding flow velocities are shown in Tables A.6-A.9. It is noted that in this and the following sections the terms "catenary riser" and "SCR riser" (usual industry abbreviation for steel catenary riser) will be used interchangeably and will refer to the catenary riser used in the NDP experiments.

3.5.1 Incidence angle: 0 deg

In this case, the incidence angle between the catenary plane and the incoming flow stream was 0 deg, i.e. the catenary plane was aligned with the flow. The results for the amplitude prediction are shown in Figure 3-13.

As is evident in Figure 3-13, the extracted optimal parametric hydrodynamic coefficient database can very accurately predict the amplitude response of the SCR riser. Not only the amplitude is predicted to errors on average (accross the span) of less than 20% (and much better in almost all cases), the mode number and shape is also very well predicted. The amplitude variation is also predicted to great accuracy.

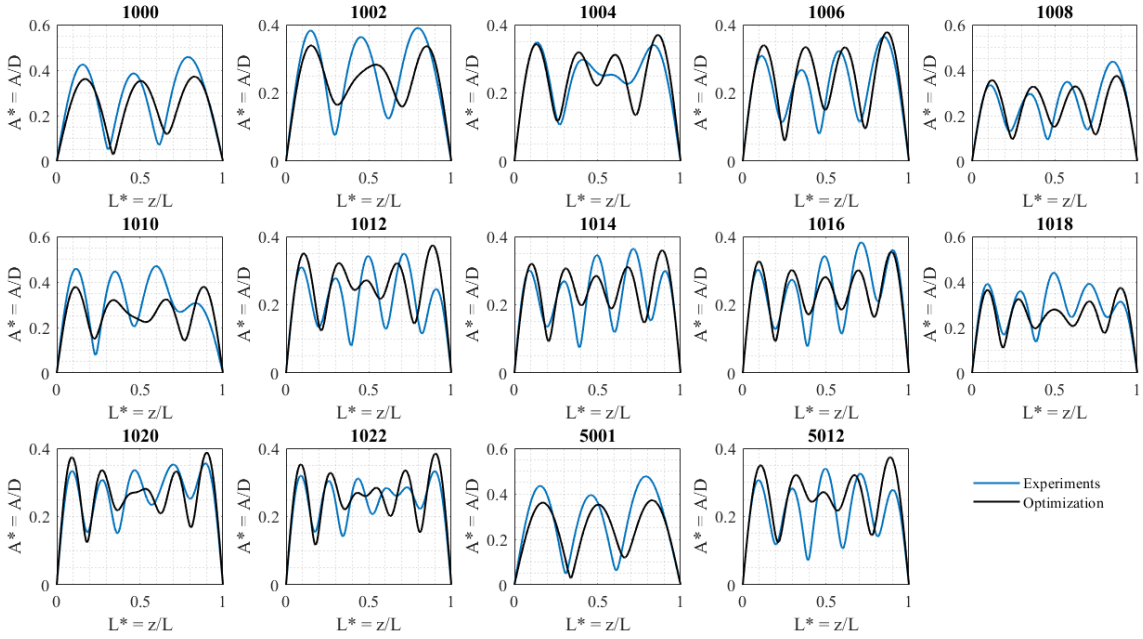

Figure 3-13: Amplitude prediction for SCR riser at 0 deg incidence angle between the catenary plane and the incoming flow

In the case of the SCR riser, the mode number is very clear in both the observed response as well as the predictions.

The frequency response is shown in Figure 3-14. As figure 3-14 illustrates, the frequency response is not predicted as well as the amplitude response is. In terms of absolute magnitude the predicted frequencies are less than a single unit off compared to predictions, however, in relative terms the error can be as high as 25-30%. It appears as if the trend of the observed data isn't very well captured by the prediction. The predicted frequency "jumps" correspond to an increase in the mode number of the amplitude response and are expected in theory. For example from a steam velocity $U = 0.14$ m/s (exp. no. 1002) to $U = 0.16$ m/s (exp. no. 1004) the mode number changes from 3 to 4 and a frequency "jump" is expected in theory. The observed results however show a more gradual (almost linear) increasing trend in the frequency.

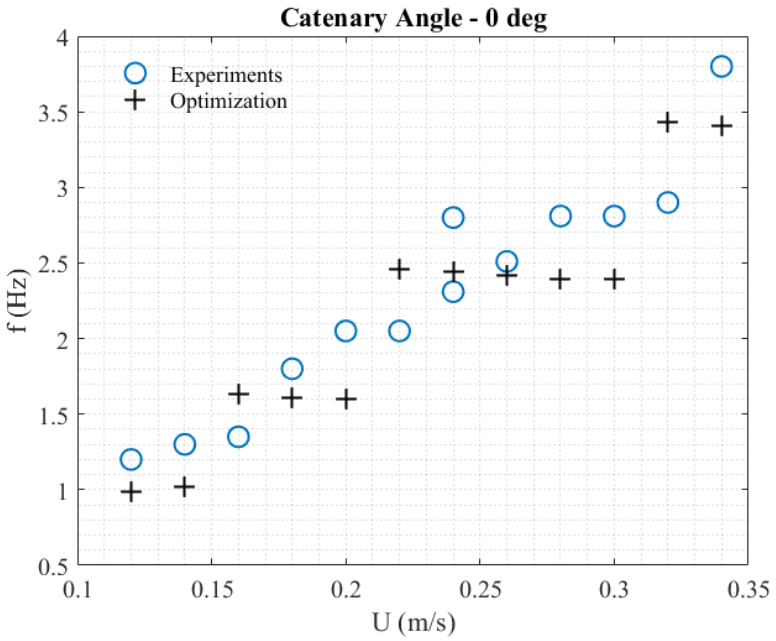

Figure 3-14: Frequency prediction for SCR riser at 0 deg incidence angle between the catenary plane and the incoming flow

3.5.2 Incidence angle: 30 deg

In this case, the incidence angle between the catenary plane and the incoming flow stream was 30 deg. Balooning effects as well as curvature effects are superimposed. Note that the CF direction remains unchanged and is defined as the direction perpendicular to the flow, rather than the direction perpendicular to the catenary plane. The amplitude response of the SCR riser at a 30 deg incidence angle between the catenary plane and the flow is shown in Figure 3-15.

As is evident in Figure 3-15, the hydrodynamic coefficient database obtained after completing the learning problem on the 30 deg incidence angle data set is competent in predicting the amplitude response of the SCR riser both in terms of amplitude in terms of mode number. The mode shape is also accurately predicted. Specifically, on a spanwise average basis the amplitude is predicted to an error of less than 20% at most and the amplitude variation evident in the observed responses is also well predicted. The mode number is correctly predicted to within 1 in all cases. In addition, the asymmetry of the response which was expected in the experiments since

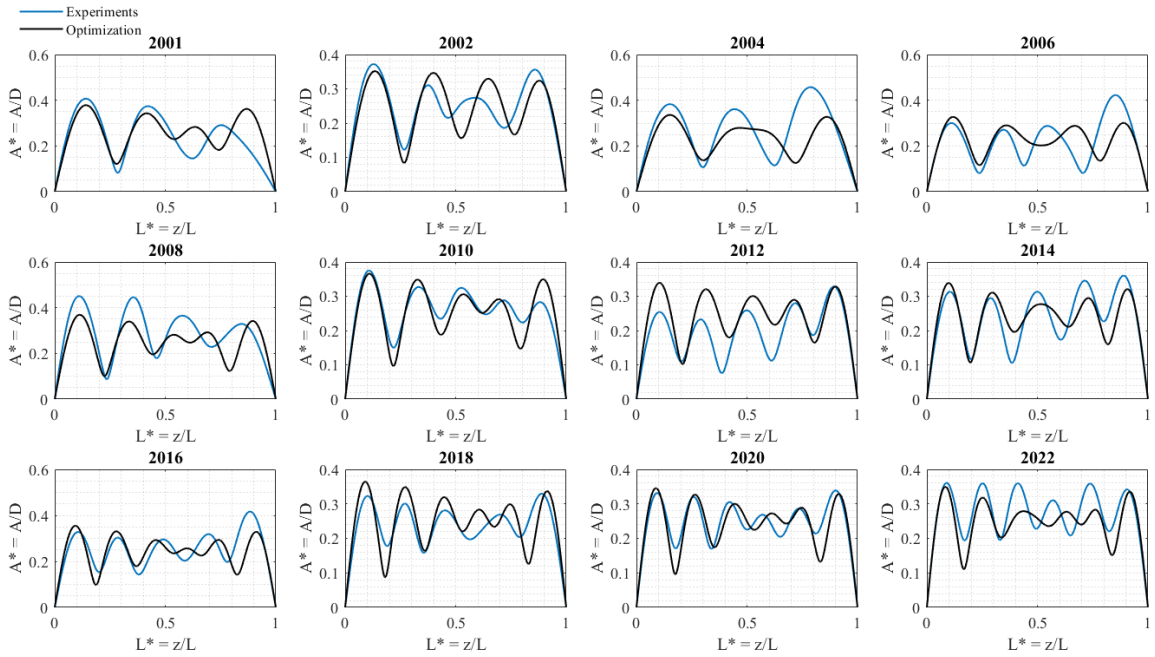

Figure 3-15: Amplitude prediction for SCR riser at 30 deg incidence angle between the catenary plane and the incoming flow

the flow velocity as seen by the riser changes as a function of its span is well captured by the reduced order model with peak location prediced to errors of less than 10% in most cases. The frequency response results are shown in Figure 3-16.

As Figure 3-16 illustrates, the frequency prediction agrees well with the experimental observations. The two discrepancies for flow velocities $U = 0.20$ m/s and $U = 0.22$ m/s are outlier points and are probably caused by a fault in measurement. However, it was decided to not exclude them from the predictions or the training process to see how outlier points affect the training, which was also done a second time excluding the outliers. With the nature of the forward model being physics-based, the prediction with or without the outliers was almost the same. That serves as evidence that, given its physics-based and physics-informed nature, the model doesn't easily overfit during training.

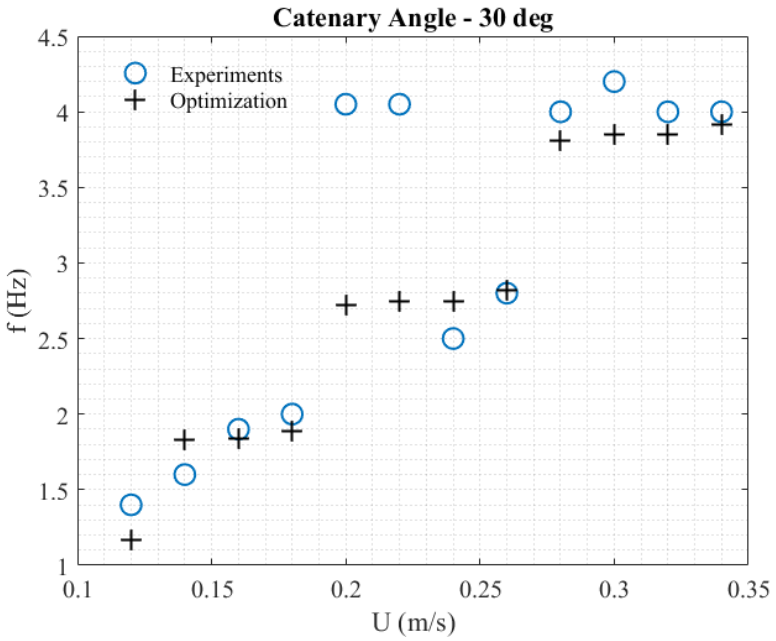

Figure 3-16: Frequency prediction for SCR riser at 30 deg incidence angle between the catenary plane and the incoming flow

3.5.3 Incidence angle: 60 deg

In this case, the incidence angle between the catenary plane and the incoming flow stream was 60 deg. Again, balooning effects as well as curvature effects were present. Note that the CF direction remains unchanged and is defined as the direction perpendicular to the flow, rather than the direction perpendicular to the catenary plane.

The amplitude response of the SCR riser at a 60 deg incidence angle between the catenary plane and the flow is shown in Figure 3-17. As Figure 3-17 illustrates, the amplitude prediction of the optimized database matches closely with the observed response from experiments. On average the response amplitude is predicted with errors of less than 20% (and much lower in most cases) with the mode number consistently predicted to within 1. The mode shape as well as the amplitude variation across the span are also well predicted with variances of the predicted and observed responses being comparable. Finally, the peak locations in most cases are correctly predicted to errors of less than 15% although there are some exceptions. The observed asymmetry is also predicted by the trained forward model and in this case the asymetry manifests

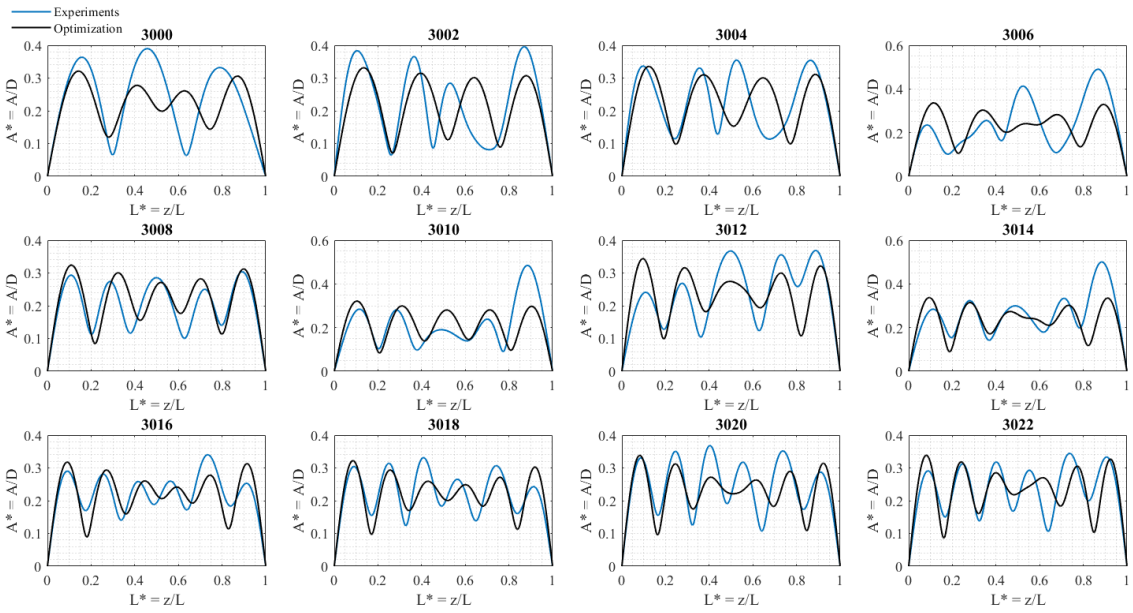

Figure 3-17: Amplitude prediction for SCR riser at 60 deg incidence angle between the catenary plane and the incoming flow

itself as an asymetry of the peak loactions although amplitude magnitude differences are also present.

Figure 3-18 shows the frequency responses for this data set. As is evident in the figure, the frequency is well predicted by the reduced order model using the trained parametric hydrodynamic coefficient database. In all cases, the response is predicted with an error of less than 15% and in most cases the relative error does not exceed 5%. Moreover, the frequency "jumps" observed, which correspond to increases in the mode number of the amplitude response, were also accurately predicted. Two mode increases are present in Figure 3-20, occurring between $U = 0.18$ m/s and $U = 0.20$ m/s (from fourth to fifth mode), as well as between $U = 0.26$ m/s and $U = 0.28$ m/s (from fifth to sixth mode); the mode "jumps" may also be seen in Figure 3-17.

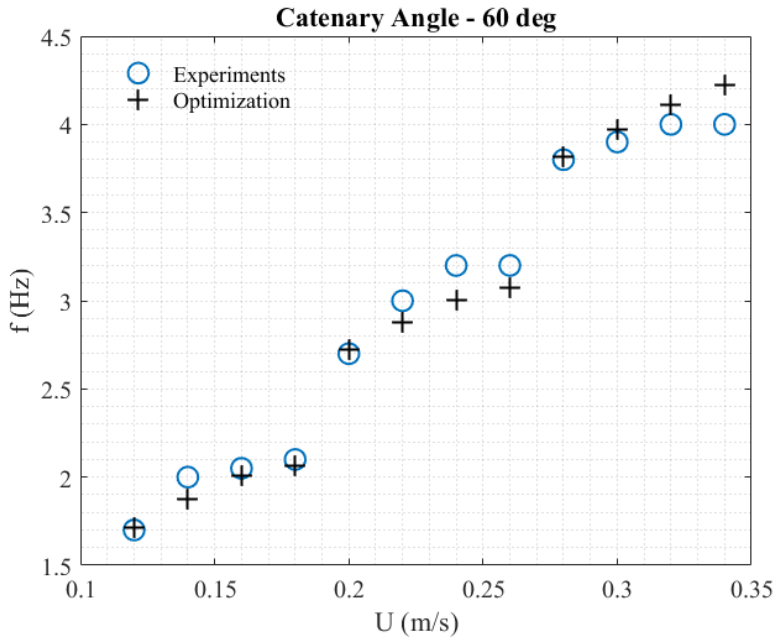

Figure 3-18: Frequency prediction for SCR riser at 60 deg incidence angle between the catenary plane and the incoming flow

3.5.4 Incidence angle: 90 deg

In this case, the catenary plane orientation with respect to the incoming flow stream was at right angles; thus, the cross-flow direction is oriented parallel to the catenary plane and balooning effects are maximized. It should be noted that since the catenary plane and the incoming flow are at right angles, the velocity as seen by the riser across the span is constant; only minor asymmetries could arise due to the curvature which is unsymmetrical. Thus, the predicted responses are almost perfectly symmetric and although not perfectly, as expected, the observed responses from experiments are also symmetric, especially for the higher flow velocities.

The results for the amplitude prediction are shown in Figure 3-19. As is illustrated in Figure 3-19 both the magnitude of the response as well as the mode number are accurately predicted in most cases. The amplitude on a spanwise average basis is predicted to a relative error of less than 10% and observed spanwise variations are also predicted. The mode shape and peak locations are also predicted to within 20% of their true locations (and to within 10% in many cases) although some ex-

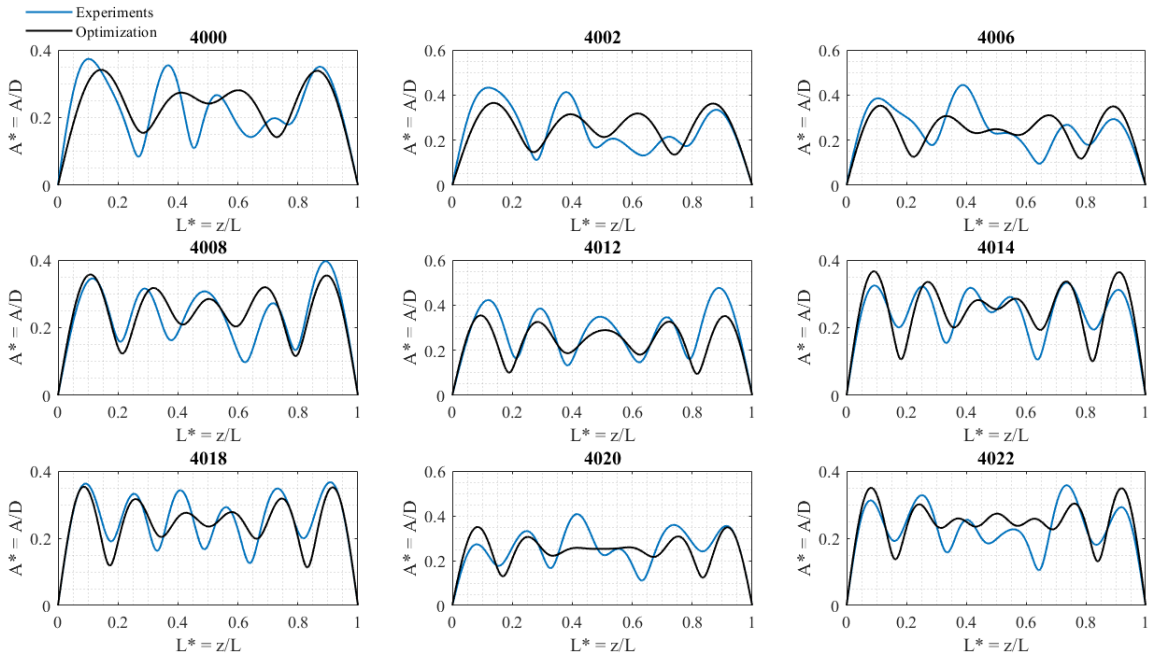

Figure 3-19: Amplitude prediction for SCR riser at 90 deg incidence angle between the catenary plane and the incoming flow

ceptions do exist. For example, in cases which experimental results show significant asymmetry, such as case "4000" (with the asymmetry arising due to imperfections in the setup combined with a low flow velocity, similar to the asymmetries observed in the symmetric uniform flow problem rather than a real asymmetry of the problem) peak locations are not very well predicted. For higher flow velocities however the asymmetries become much less apparent.

The frequency responses are shown in Figure 3-20. The observed frequencies from experiments are well predicted by the forward model after training. For flow velocities less than $U = 0.25$ m/s the predictions match observation to a relative error of less than 10%. The velocities at which the mode "jumps" occur, at $U \approx 0.15$ m/s (from 4 to 5 mode) and $U \approx 0.25$ m/s approximately (from 5 to 6 mode), are also correctly predicted. For higher flow velocities, where $U > 0.25$, the model is slightly under-predicting the frequency, by about 8-10% with the exception of $U = 0.27$ m/s where the relative error is about 13%.

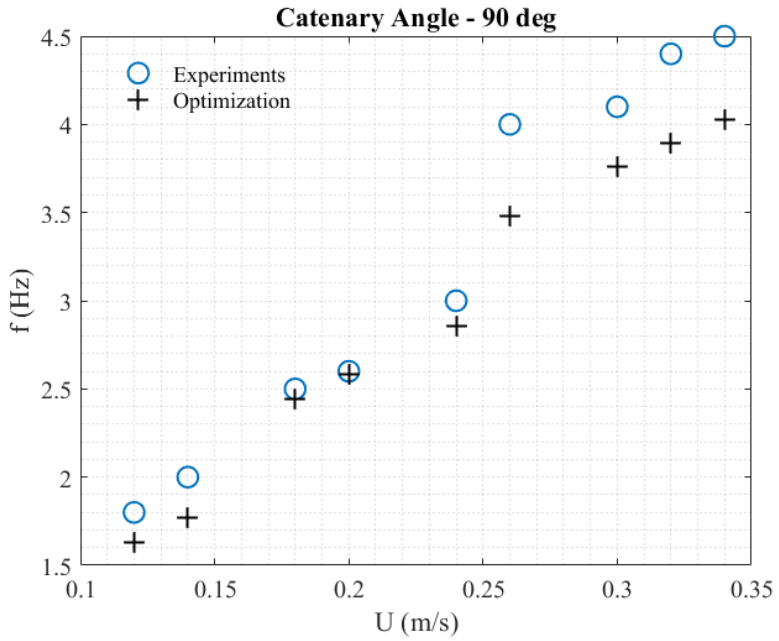

Figure 3-20: Frequency prediction for SCR riser at 90 deg incidence angle between the catenary plane and the incoming flow

3.6 Stepped flexible riser in uniform flow

Relatively few things are known about VIV of cylinders with distinct diameters across the span. For the purpose of this work, experimental data obtained at MIT by Professor Dixia Fan as part of his PhD thesis work in 2019 were used. A flexible cylinder with two distinct diameters measuring $d = d_1 = 5$ mm and $d_2 = 8$ mm each spanning half the cylinder's total length of $L = 1.22$ m was used. The particulars of the riser model are detailed in Table A.10. Figure B-3 aims to help the reader visualize the test setup.

The structural response as Fan reports[13] is complex in the sense that as work via wavelet synchrosqueezed transform reveals, two **distinct frequency vibrations coexist on the structure at the same time**. Two distinct travelling wave responses are induced on the cylinder (initiated at the two distinct diameter regions) and propagate along the structure.

In order to account for the two distinct frequency coexisting vibrations, two parametric hydrodynamic coefficient databases were used. Although the two databases

were of the same parametric form (as described in Section 2.2.2), each was used to predict a separate half of the riser (corresponding to a separate diameter). Training of the two databases was done according to Equation 2.24 in a sequential fashion, optimizing each database given the other constant and alternating between the two. Therefore, in order to solve Equation 2.10 to obtain the amplitude and frequency response a distinct parametric hydrodynamic coefficient database was used for each half of the riser making the problem highly nonlinear. The identified dominant and subdominant response frequencies (which need not be multiples of each other since solutions to 2.10 need not be mutually orthogonal) were used to predict the two distinct observed frequencies.

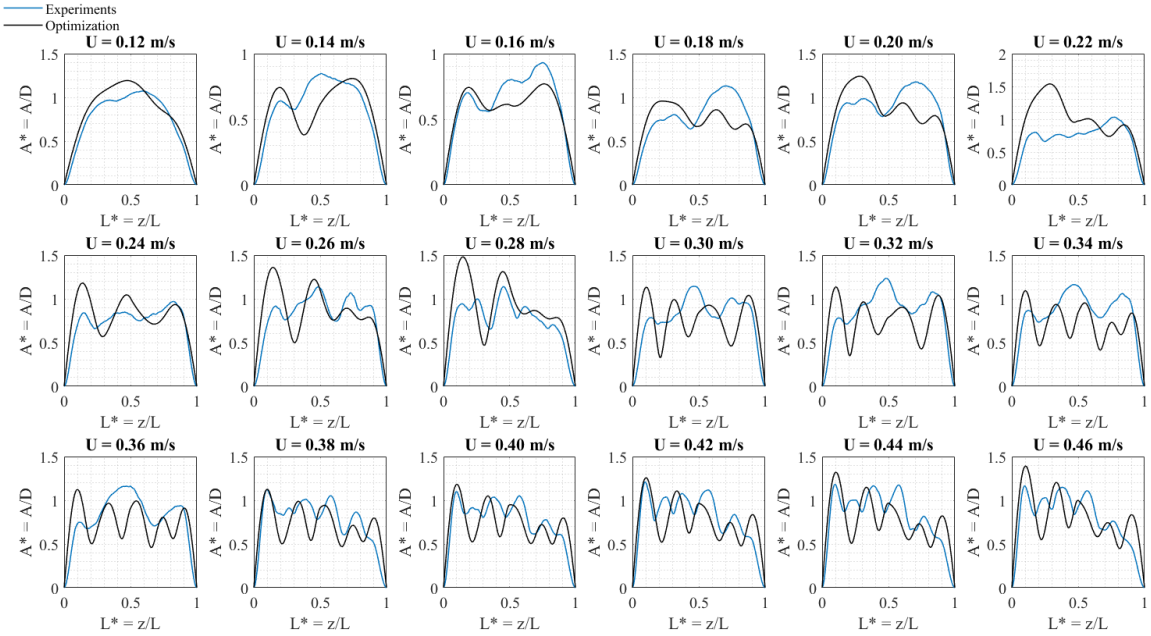

Figure 3-21: Amplitude prediction for Step "5-8" riser

Figure 3-21 illustrates the predicted amplitude response (as a solid black line) along with the observed response (as a solid blue line). As expected the amplitude responses are highly asymmetric. Although the observed responses deviate in some cases from the predicted ones, the overall shape and trend of the response is captured and the magnitude is adequately approximated; the average error across the span is less than 20% in about half the cases; in those cases the mode shape and mode number

are also adequately predicted. There exists a window of flow velocities $U \in [0.30, 0.36]$ in which the observed and predicted response deviate significantly in trend, mode number, and amplitude.

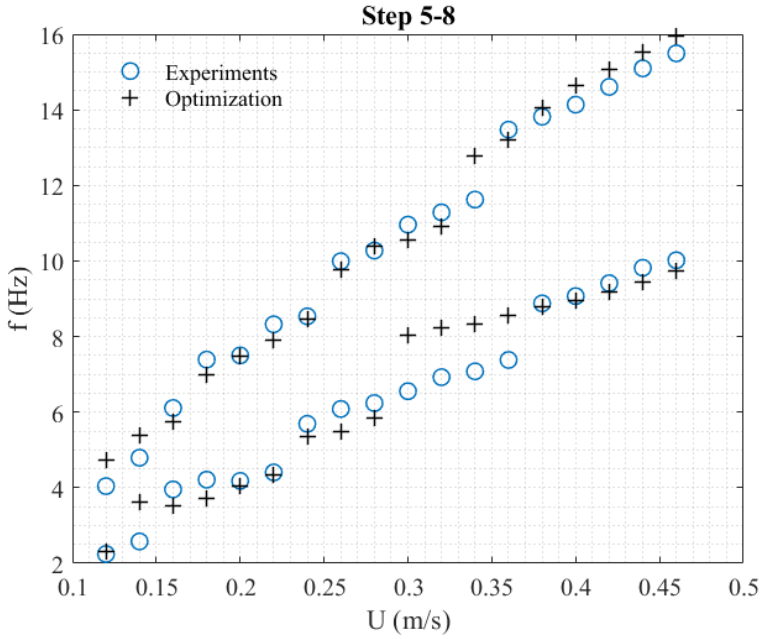

Figure 3-22: Frequency prediction for Step "5-8" riser

Figure 3-22 shows the two distinct frequency predictions as well as the experimentally measured ones. As is evident in the figure, the trained model can very accurately predict both frequencies in most cases with the exception of the low frequencies at $U \approx 0.3$ m/s up to $U \approx 0.35$ m/s. This is a transition region between modes as is evident in Figure 3-21 which is not accurately predicted by the forward model after training. However, besides that region, the trained model does well in terms of predicting the two distinct coexisting frequencies, which are not multiples of each other, i.e. the modes solving Equation 2.10 are not orthogonal. The predictions are accurate to to a relative error of less than 10% in all cases outside the transition region.

The step cylinder results show that the non-orthogonal modes predicted in theory do indeed show up in experimental applications, further validating the forward model. Applying the methodology to the Step "5-8" riser is an ambitious goal and although far from perfect, the results are promising. Perhaps with appropriate modifications

of the learning problem, the complex flow structure interaction may be not only be well predicted but also further understood.

Chapter 4

Conclusions

4.1 Research summary

Accurate prediction of the structural response of flexible bodies in VIV relies heavily on the quality of the obtained hydrodynamic coefficient database used to solve the coupled flow/structure interaction problem. Traditionally, databases were obtained via rigid-cylinder forced vibration experiments, a method not only very expensive and time consuming but also limited in the sense it only allows for the inference of databases for very specific flow conditions and body geometries. Computational fluid dynamics simulations are not yet capable of resolving full scale risers ($L/D = O(10^4)$) at field operating Reynolds numbers ($Re = O(10^5)$). There exists thus a need for developing a methodology to infer databases which may be used not only to make accurate predictions but also to illuminate the underlying principles which govern VIV.

The methodology presented in this work provides an alternative way of studying vortex induced vibrations of flexible structures, by machine-learning the hydrodynamic coefficients used to solve the coupled flow/structure interaction problem from experimental data. The proposed framework is applied to a uniform flexible cylinder in uniform flow, and then extended to a uniform cylinder in a stepped current and a sheared current. Furthermore, it is applied to a catenary flexible cylinder, as well as a stepped (2 diameter) flexible cylinder. Last but not least, the framework is extended

to using *direct sparse sensor measurements* along the structure instead of (virtually unlimited) reconstructed displacement measurements.

The extracted database from each individual data set is used to make predictions of the amplitude and frequency response observed experimentally. The predictions are in most cases accurate to errors of less than 15-20% of the observed amplitude (on average accross the span) and less than 10-20% of the observed frequency of vibration.

4.2 Recommendations for future research

The methodology presented in this work was originally proposed by Rudy et al.[27]. It is further validated and extended to non-uniform incoming flow profiles as well as non-uniform riser geometries. Finally, the framework is extended to using direct sparse sensing. The study reveals that there is a lot of potential in the capabilities of the methodology in terms of increasing the predictive accuracy of semi-empirical models. The predictions of the forward model using the extracted hydrodynamic databases compare with those of much higher complexity, high fidelity models (and are perhaps even superior after training).

Although the methodology is extended to using direct sparse sensing for a uniform riser in uniform flow, it remains to be further validated to non-uniform riser geometries and non-uniform incoming flow profiles using direct sparse sensing. Additional directions that should be explored are determining the optimal sensor number and associated placement along the body's span in order to obtain an accurate reconstruction of the body's response with the least amount of data.

Furthermore, additional work could be done towards developing the optimization algorithm. Currently, a stochastic coordinate descent method is employed to search the parametric space and return the optimal parametric database. The optimization takes approximately 12-24 hours to complete for $O(10)$ GB databases. As discussed in Chapter 2, various reasons led to avoiding gradient methods given the chosen parametric form. However, perhaps different optimization algorithms could improve the wall time of the program and additionally, an alternative choice of parametrization

might allow for reconsidering other algorithms. The geometry of the objective function (Equation 2.24) also remains to be explored: does it accept a unique global optimum? perhaps more than one non-unique optima? Could the algorithm used in this work be "stuck" in a local optimum rather than landing on the global one (if it exists)? Additionally, examining the effect of the regularization terms on the objective function, as well as exploring alternative regularizations are directions to be explored. Penalizing the variation of the amplitude response is a strongly recommended direction.

Although this is a low-fidelity (reduced order) model it may be used as part of multi-fidelity modelling. Provided one or more additional predictions of the flexible body's response, the results from this model could be used together with the other predictions to obtain even better estimates of the body's response. Field measurements of risers are notoriously difficult to obtain. Not only they are confidential but in most cases the sensors along the span are not enough to reconstruct the body's motion with significant confidence. The proposed methodology is yet to be applied to field data and its ability to reproduce well understood results remains to be tested.

Finally, exploring what can be learned from the inferred databases in terms of VIV hydrodynamics remains to be explored. Whether obtaining a universal hydrodynamic coefficient database (in the sense of making accurate predictions across various riser geometries and flow conditions) is possible, and "how universal" would such a database be also remains an open question.

Appendix A

Tables

Table A.1: NDP uniform riser specifications

Riser Specification	**Value**
Material	Fiberglass
Length	38 m
Outer diameter	27 mm
Length to diameter ratio	1407
Wall thickness of pipe	3.0 mm
Flexural rigidity (EI)	37.2 Nm^2
Young's modulus (E)	$3.62 \cdot 10^{10}$ $\mathrm{N/m}^2$
Axial stiffnes (EA)	$5.09 \cdot 10^{5}$ N
Mass (water filled)	0.933 kg/m
Mass ratio	1.62

Table A.2: NDP uniform test numbers

Test number	**Flow velocity**
2010	0.3 m/s
2020	0.4 m/s
2030	0.5 m/s
2040	0.6 m/s
2050	0.7 m/s
2060	0.8 m/s
2070	0.9 m/s
2080	1.0 m/s
2090	1.1 m/s
2100	1.2 m/s
2110	1.3 m/s
2120	1.4 m/s
2130	1.5 m/s
2141	1.6 m/s
2150	1.7 m/s
2160	1.8 m/s
2170	1.9 m/s
2182	2.0 m/s
2191	2.1 m/s
2201	2.2 m/s
2210	2.3 m/s
2220	2.4 m/s

Table A.3: Chaplin et al.[8] riser specifications

Riser Specification	**Value**
Length	13.12 m
Outer diameter	28 mm
Length to diameter ratio	468
Flexural rigidity (EI)	29.9 Nm^2
Weight	12.1 N/m
Mass ratio	3

Table A.4: NDP shear test numbers

Test number	**Flow velocity**
2310	0.3 m/s
2320	0.4 m/s
2330	0.5 m/s
2340	0.6 m/s
2350	0.7 m/s
2360	0.8 m/s
2370	0.9 m/s
2380	1.0 m/s
2390	1.1 m/s
2400	1.2 m/s
2410	1.3 m/s
2420	1.4 m/s
2430	1.5 m/s
2440	1.6 m/s
2450	1.7 m/s
2460	1.8 m/s
2470	1.9 m/s
2480	2.0 m/s
2490	2.1 m/s
2500	2.2 m/s
2510	2.3 m/s
2520	2.4 m/s

Table A.5: NDP catenary (SCR) riser specifications

Riser Specification	**Value**
Material	Brass
Length	12.5 m
Outer diameter	14 mm
Wall thickness of pipe	0.45 mm
Flexural rigidity (EI)	46.2 Nm^2
Young's modulus (E)	$1.05 \cdot 10^{11}$ N/m^2
Axial stiffnes (EA)	$2.01 \cdot 10^6$ N
Mass (including content)	0.357 kg/m
Horizontal distance between ends	9.253 m
Vertical distance between ends	7.130 m
Tension, upper end	22.55 N
Tension, lower end	8.44 N
Angle from vertical, upper end	26 deg
Angle from vertical, lower end	88 deg

Table A.6: NDP SCR 0 deg test numbers

Test number	**Flow speed**
1000 & 1001 & 5001 & 5002	0.12 m/s
1002 & 1003	0.14 m/s
1004 & 1005	0.16 m/s
1006 & 1007	0.18 m/s
1008 & 1009	0.20 m/s
1010 & 1011	0.22 m/s
1012 & 1013 & 5012 & 5013	0.24 m/s
1014 & 1015	0.26 m/s
1016 & 1017	0.28 m/s
1018 & 1019 & 5018 & 5019	0.30 m/s
1020 & 1021	0.32 m/s
1022 & 1023 & 5022 & 5023	0.34 m/s

Table A.7: NDP SCR 30 deg test numbers

Test number	**Flow speed**
2004 & 2005	0.12 m/s
2000 & 2001	0.14 m/s
2002 & 2003	0.16 m/s
2006 & 2007	0.18 m/s
2008 & 2009	0.20 m/s
2010 & 2011	0.22 m/s
2012 & 2013	0.24 m/s
2014 & 2015	0.26 m/s
2016 & 2017	0.28 m/s
2018 & 2019	0.30 m/s
2020 & 2021	0.32 m/s
2022 & 2023	0.34 m/s

Table A.8: NDP SCR 60 deg test numbers

Test number	**Flow speed**
3000 & 3001	0.12 m/s
3002 & 3003	0.14 m/s
3004 & 3005	0.16 m/s
3006 & 3007	0.18 m/s
3008 & 3009	0.20 m/s
3010 & 3011	0.22 m/s
3012 & 3013	0.24 m/s
3014 & 3015	0.26 m/s
3016 & 3017	0.28 m/s
3018 & 3019	0.30 m/s
3020 & 3021	0.32 m/s
3022 & 3023	0.34 m/s

Table A.9: NDP SCR 90 deg test numbers

Test number	**Flow speed**
4000 & 4001	0.12 m/s
4002	0.14 m/s
4005	0.16 m/s
4006 & 4007	0.18 m/s
4008	0.20 m/s
4011	0.22 m/s
4012 & 4013	0.24 m/s
4014	0.26 m/s
4017	0.28 m/s
4018 & 4019	0.30 m/s
4020 & 4021	0.32 m/s
4022 & 4023	0.34 m/s

Table A.10: Step "5-8" riser specifications

Riser Specification	**Value**
Material	Urethane & tungsten powder
Length	1.22 m
First diameter $d = d_1$	5 mm
Second diameter d_2	8 mm
Aspect Ratio L/d	244

Appendix B

Figures

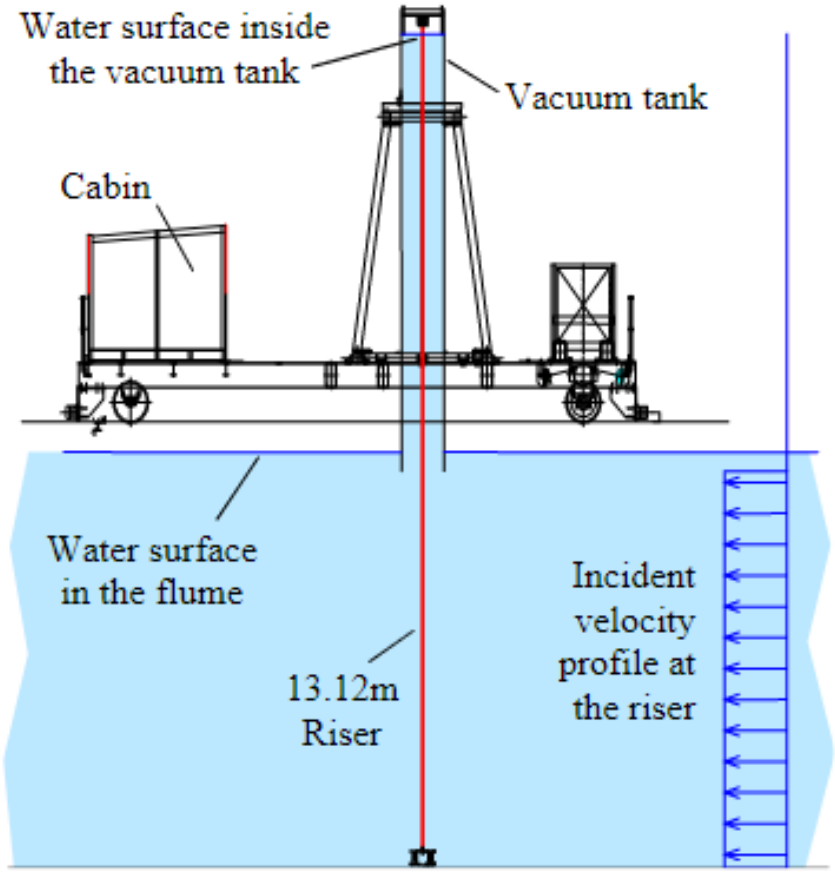

Figure B-1: Experimental layout for straight riser in stepped current. Adapted from [8]

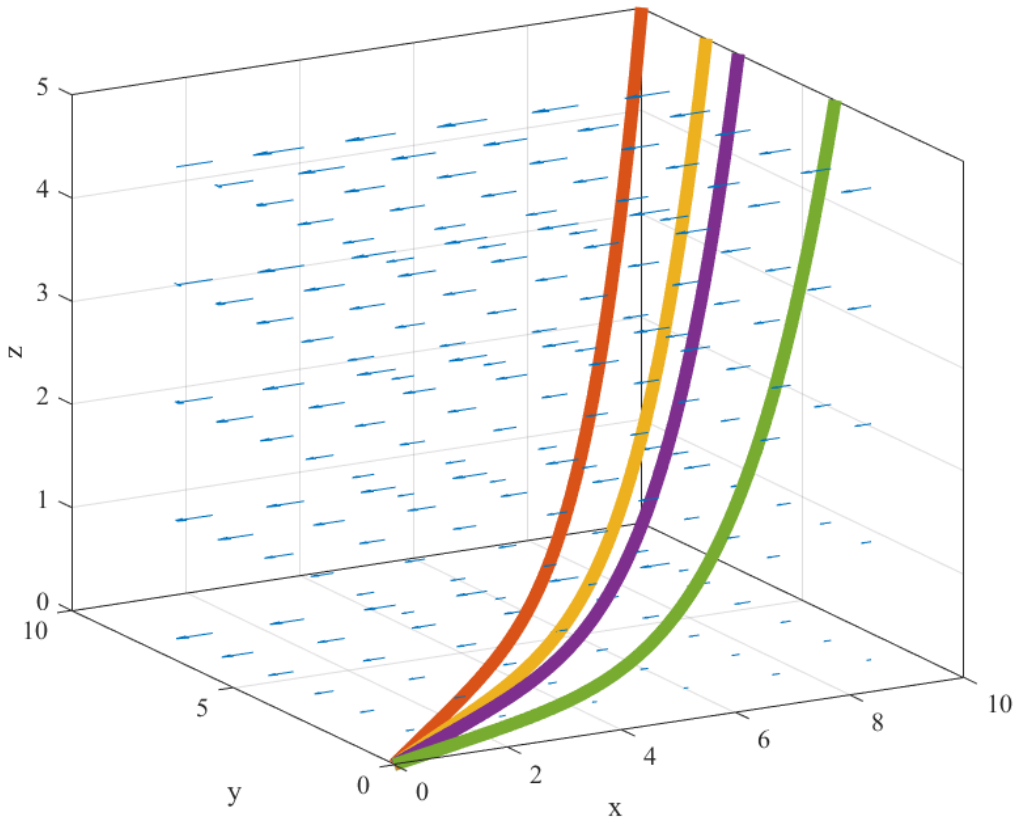

Figure B-2: Visualization of the catenary riser

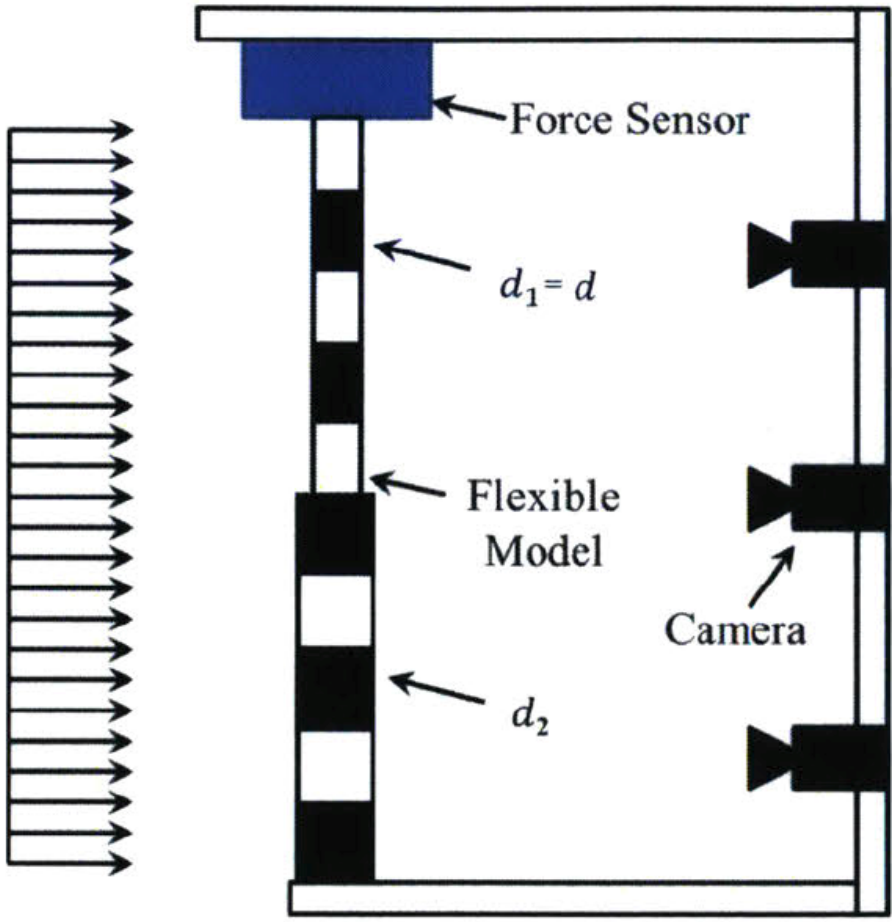

Figure B-3: Step "5-8" cylinder setup. Adapted from [14]

Bibliography

[1] Hyoungsu Baek and George Em Karniadakis. Suppressing vortex-induced vibrations via passive means. *Journal of Fluids and Structures*, 25(5):848–866, 2009.

[2] Michael M Bernitsas. Harvesting energy by flow included motions. In *Springer handbook of ocean engineering*, pages 1163–1244. Springer, 2016.

[3] Michael M Bernitsas, Y Ben-Simon, Kamaldev Raghavan, and EMH Garcia. The vivace converter: model tests at high damping and reynolds number around 105. *Journal of offshore mechanics and Arctic engineering*, 131(1), 2009.

[4] Michael M Bernitsas, James Ofuegbe, Jau-Uei Chen, and Hai Sun. Eigen-solution for flow induced oscillations (viv and galloping) revealed at the fluid-structure interface. In *ASME 2019 38th International Conference on Ocean, Offshore and Arctic Engineering*. American Society of Mechanical Engineers Digital Collection, 2019.

[5] Michael M Bernitsas and Kamaldev Raghavan. Reduction/suppression of viv of circular cylinders through roughness distribution at 8× 103< re< 1.5× 105. In *International Conference on Offshore Mechanics and Arctic Engineering*, volume 48227, pages 1001–1005, 2008.

[6] Michael M Bernitsas, Kamaldev Raghavan, Y Ben-Simon, and EMH Garcia. Vivace (vortex induced vibration aquatic clean energy): A new concept in generation of clean and renewable energy from fluid flow. *Journal of offshore mechanics and Arctic engineering*, 130(4), 2008.

[7] Henning Braaten and Halvor Lie. Ndp riser high mode viv tests main report. *MARINTEK report, Trondheim, Norway*, 2005.

[8] JR Chaplin, PW Bearman, FJ Huera Huarte, and RJ Pattenden. Laboratory measurements of vortex-induced vibrations of a vertical tension riser in a stepped current. *Journal of Fluids and Structures*, 21(1):3–24, 2005.

[9] Lin Ding, Michael M Bernitsas, and Eun Soo Kim. 2-d urans vs. experiments of flow induced motions of two circular cylinders in tandem with passive turbulence control for 30,000< re< 105,000. *Ocean Engineering*, 72:429–440, 2013.

[10] Wenjun Ding, Hai Sun, Wanhai Xu, and Michael M Bernitsas. Numerical investigation on interactive fio of two-tandem cylinders for hydrokinetic energy harnessing. *Ocean Engineering*, 187:106215, 2019.

[11] C Evangelinos, D Lucor, and GE Karniadakis. Dns-derived force distribution on flexible cylinders subject to vortex-induced vibration. *Journal of fluids and structures*, 14(3):429–440, 2000.

[12] D. Fan, G. Jodin, T. R. Consi, L. Bonfiglio, Y. Ma, L. R. Keyes, G. E. Karniadakis, and M. S. Triantafyllou. A robotic intelligent towing tank for learning complex fluid-structure dynamics. *Sci. Robot.*, 4(36), 2019.

[13] Dixia Fan. *Mapping the hydrodynamic properties of flexible and rigid bodies undergoing vortex-induced vibrations.* PhD thesis, Massachusetts Institute of Technology, 2019.

[14] Dixia Fan, Zhicheng Wang, Michael S Triantafyllou, and George Em Karniadakis. Mapping the properties of the vortex-induced vibrations of flexible cylinders in uniform oncoming flow. *Journal of Fluid Mechanics*, 881:815–858, 2019.

[15] R. Gopalkrishnan. *Vortex-induced forces on oscillating bluff cylinders.* PhD thesis, Massachusetts Institute of Technology, 1993.

[16] R Govardhan and CHK Williamson. Resonance forever: existence of a critical mass and an infinite regime of resonance in vortex-induced vibration. *Journal of Fluid Mechanics*, 473:147–166, 2002.

[17] Qinghua Han, Yexuan Ma, Wanhai Xu, Dixia Fan, and Enhao Wang. Hydrodynamic characteristics of an inclined slender flexible cylinder subjected to vortex-induced vibration. *International Journal of Mechanical Sciences*, 148:352–365, 2018.

[18] FS Hover, H Tvedt, and MS Triantafyllou. Vortex-induced vibrations of a cylinder with tripping wires. 2001.

[19] Eun Soo Kim, Hai Sun, Hongrae Park, Sung-chul Shin, Eun Jung Chae, Ryan Ouderkirk, and Michael M Bernitsas. Development of an alternating lift converter utilizing flow-induced oscillations to harness horizontal hydrokinetic energy. *Renewable and Sustainable Energy Reviews*, 145:111094, 2021.

[20] C. M. Larsen, K. Vikestad, R. Yttervik, E. Passano, and G. S. Baarholm. Vivana theory manual. *Marintek, Trondheim, Norway*, 2001.

[21] Yanfang Lv, Liping Sun, Michael M Bernitsas, and Hai Sun. A comprehensive review of nonlinear oscillators in hydrokinetic energy harnessing using flow-induced vibrations. *Renewable and Sustainable Energy Reviews*, 150:111388, 2021.

[22] TL Morse and CHK Williamson. The effect of reynolds number on the critical mass phenomenon in vortex-induced vibration. *Physics of Fluids*, 21(4):045105, 2009.

[23] Hongrae Park, R Ajith Kumar, and Michael M Bernitsas. Suppression of vortex-induced vibrations of rigid circular cylinder on springs by localized surface roughness at 3× 104≤ re≤ 1.2× 105. *Ocean Engineering*, 111:218–233, 2016.

[24] K Raghavan and MM Bernitsas. Experimental investigation of reynolds number effect on vortex induced vibration of rigid circular cylinder on elastic supports. *Ocean Engineering*, 38(5-6):719–731, 2011.

[25] Maziar Raissi, Zhicheng Wang, Michael S Triantafyllou, and George Em Karniadakis. Deep learning of vortex-induced vibrations. *Journal of Fluid Mechanics*, 861:119–137, 2019.

[26] F. E. Roveri and J. K. Vandiver. Using shear7 for assessment of fatigue damage caused by current induced vibrations. In *Proc. 20th OMAE Conf.*, pages 3–8, 2001.

[27] Samuel Rudy, Dixia Fan, Jose del Aguila Ferrandis, Themistoklis Sapsis, and Michael S Triantafyllou. Learning optimal parametric hydrodynamic database for vortex-induced crossflow vibration prediction. *arXiv preprint arXiv:2104.05887*, 2021.

[28] T. Sarpkaya. Fluid forces on oscillating cylinders. *NASA STI/Recon Technical Report A*, 78:275–290, 1978.

[29] T. Sarpkaya. Hydrodynamic damping, flow-induced oscillations, and biharmonic response. *J. Offshore Mech. Arct. Eng.*, 117(4):232–238, 1995.

[30] Turgut Sarpkaya. Vortex-induced oscillations: a selective review. 1979.

[31] M. S. Triantafyllou, G. S. Triantafyllou, Y. S. Tein, and B. D. Ambrose. Pragmatic riser viv analysis. In *Offshore Tech. Conf.* Offshore Technology Conference, 1999.

[32] JK Vandiver. Shear7 program user manual. *Massachusetts Institute of Technology, Cambridge, MA*, 1999.

[33] Jia-song Wang, Dixia Fan, and Ke Lin. A review on flow-induced vibration of offshore circular cylinders. *Journal of Hydrodynamics*, 32(3):415–440, 2020.

[34] X. Wang, R. So, and K. Chan. A non-linear fluid force model for vortex-induced vibration of an elastic cylinder. *J. Sound Vib.*, 260(2):287–305, 2003.

[35] Z. Wang, D. Fan, and M. S. Triantafyllou. Illuminating the complex role of the added mass during vortex induced vibration. *Phys. Fluids*, 33(8):085120, 2021.

[36] Z. Wang, D. Fan, M. S. Triantafyllou, and G. E. Karniadakis. A large-eddy simulation study on the similarity between free vibrations of a flexible cylinder and forced vibrations of a rigid cylinder. *J. Fluids Struct.*, 101:103223, 2021.

[37] C. H. K. Williamson. Vortex dynamics in the cylinder wake. *Annu. Rev. Fluid Mech.*, 28(1):477–539, 1996.

[38] Charles HK Williamson. Oblique and parallel modes of vortex shedding in the wake of a circular cylinder at low reynolds numbers. *Journal of Fluid Mechanics*, 206:579–627, 1989.

[39] Charles HK Williamson and R Govardhan. Vortex-induced vibrations. *Annu. Rev. Fluid Mech.*, 36:413–455, 2004.

[40] Wei Wu, Michael M Bernitsas, and Kevin Maki. Rans simulation versus experiments of flow induced motion of circular cylinder with passive turbulence control at 35,000< re< 130,000. *Journal of Offshore Mechanics and Arctic Engineering*, 136(4), 2014.

[41] Yuwang Xu, Shixiao Fu, Ying Chen, Qian Zhong, and Dixia Fan. Experimental investigation on vortex induced forces of oscillating cylinder at high reynolds number. *Ocean Systems Engineering*, 3(3):167–180, 2013.

[42] MM Zdravkovich. Different modes of vortex shedding: an overview. *Journal of fluids and Structures*, 10(5):427–437, 1996.

[43] Haining Zheng, Rachel Price, Yahya Modarres-Sadeghi, George S Triantafyllou, and Michael S Triantafyllou. Vortex-induced vibration analysis (viva) based on hydrodynamic databases. In *International Conference on Offshore Mechanics and Arctic Engineering*, volume 44397, pages 657–663, 2011.